Kinetic stability of metal–organic frameworks for corrosive and coordinating gas capture

Adam J. Rieth, Ashley M. Wright and Mircea Dincă *

Abstract | Metal–organic frameworks (MOFs) have diverse applications involving the storage, separation and sensing of weakly interacting, high-purity gases. Exposure to impure gas streams and interactions with corrosive and coordinating gases raises the question of chemical robustness; however, the factors that determine the stability of MOFs are not fully understood. Framework materials have been previously categorized as either thermodynamically or kinetically stable, but recent work has elucidated an energetic penalty for porosity for all these materials with respect to a dense phase, which has implications for the design of materials for gas storage, heterogeneous catalysis and electronic applications. In this Review, we focus on two main strategies for stabilization of the porous phase — using inert metal ions or increasing the heterolytic metal–ligand bond strength. We review the progress in designing robust materials for the capture of coordinating and corrosive gases such as H_2O vapour, NH_3, H_2S, SO_2, nitrogen oxides (NO_x) and elemental halogens. We envision that the pursuit of strategies for kinetic stabilization of MOFs will yield increasing numbers of robust frameworks suited to harsh conditions and that short-term stability towards these challenging gases will be predictive of long-term stability for applications in less demanding environments.

Porosity is a useful and versatile material property for a range of applications, including gas storage[1–4], chemical separations[5–7], catalysis[8–10] and electronic devices[11,12]. However, the empty voids of porous materials also give rise to the possibility of collapse, which is detrimental to practical applications. Metal–organic frameworks (MOFs) consist of regular arrays of metal ions or clusters linked by organic ligands and can exhibit record internal surface areas[13]. Research into MOFs and, concomitantly, the number of possible applications for these materials has increased exponentially over the past several years. However, they are not yet widely applied in industry and, in many cases, the deployment of MOFs is held back by a lack of long-term stability under environmental or application-specific conditions. In this Review, we focus on the chemical stability of frameworks towards coordinating and corrosive gases and vapours, including H_2O vapour, NH_3, H_2S, Cl_2, Br_2, nitrogen oxides (NO_x) and SO_2, which may be present in the atmosphere or components in applications for which MOFs find utility.

The energetic penalty for porosity

Horror vacui, a phrase attributed to Aristotle and roughly translated as nature abhors a vacuum, was, until recently, thought to apply to the crystallization of permanently porous solids. Porous solids were believed to be unstable, owing to the relative lack of bonding or dispersive interactions within or between the voids[14]. However, porous materials such as zeolites and MOFs are now commonly synthesized, normally by including solvent, a surfactant or structure-directing agents within the voids during crystallization, although the degree of kinetic or thermodynamic control responsible for their formation is still under debate[15]. After the porous material is synthesized, the components within the pores are commonly removed by evacuation or annealing, leaving behind accessible voids. However, an increasing body of work suggests that crystalline porous materials with empty pores are metastable with respect to their dense phases[16–21] (FIG. 1). The dense phase is a hypothetical assemblage of the same constituent atoms, ions or ligands but has negligible porosity. For an all-silica zeolite, the dense phase is easily envisaged as non-porous amorphous silica, which can be accessed by heating. For a MOF, the dense phase can be more difficult to conceptualize, owing to the directionality of the ligands, but denser amorphous phases of some MOFs, achieved thermally[22–25] or through the application of pressure[26–28], are known.

The metastability of solvent-free, porous materials has been experimentally demonstrated for many

Department of Chemistry, Massachusetts Institute of Technology, Cambridge, MA, USA.

**e-mail: mdinca@mit.edu*

https://doi.org/10.1038/s41578-019-0140-1

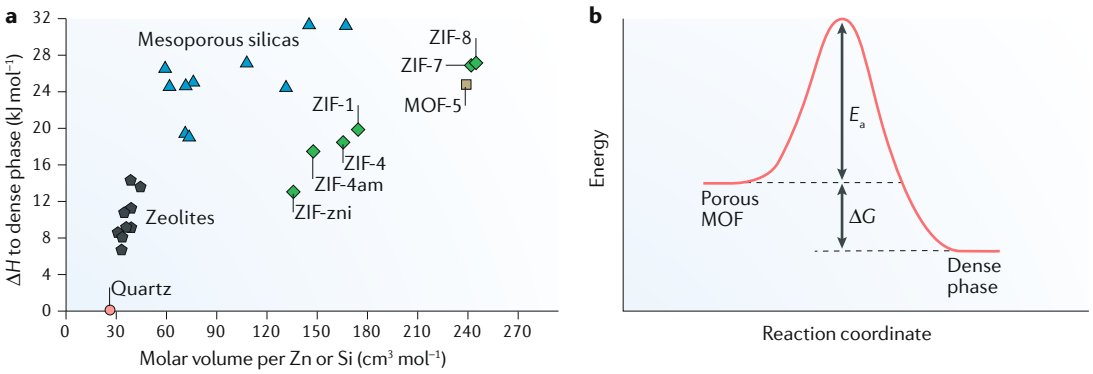

Fig. 1 | **Metastability of porous materials. a** | Plot of the enthalpic penalty (ΔH) relative to a dense phase versus the molar unit cell volume per Zn or Si for porous materials, including zeolites, mesoporous silicas, zeolitic imidazolate frameworks (ZIFs) and metal–organic framework (MOF)-5. Data from REFS[16,17,20]. **b** | Conceptualization of the energy penalty for porosity in a reaction coordinate diagram. ΔG, change in the Gibbs free energy; E_a, activation energy. Panel **a** is adapted with permission from REF.[17], ACS.

zeolites[19], zeolitic imidazolate frameworks (ZIFs)[17] and the prototypical MOFs $Zn_4O(BDC)_3$ (MOF-5; BDC^{2-} = 1,4-benzenedicarboxylate)[16] and $Cu_3(BTC)_2$ (HKUST-1; BTC^{3-} = 1,3,5-benzenetricarboxylate)[18]. Calorimetric measurements with HKUST-1 showed that the inclusion of solvent within the MOF can thermodynamically stabilize the porous phase (with respect to the dense phase)[18], whereas the inclusion of solvent for MOF-5, although highly exothermic[21], is insufficient to result in net stabilization[16]; nevertheless, for most applications, the evacuated phase is desired. It has been argued that the increased vibrational entropy of porous phases of MOFs could provide enough energetic stabilization to result in a net negative free energy with respect to dense phases at slightly elevated temperatures[15]. However, the available calorimetric data indicate a trend of increasing energy penalty for increasingly porous structures, and a dense, amorphous phase should be entropically favoured over a crystalline porous phase, given that the driving force for crystallization is typically enthalpic[20].

Stabilizing the porous MOF phase

Conceptualizing MOFs with empty pores as metastable, kinetically trapped phases has implications for the design of chemically stable frameworks: stabilization of the porous phase can only be kinetic and must increase the energy barrier for transitioning to the dense phase by either increasing the transition-state energy or decreasing the energy of the porous phase with respect to the transition state (FIG. 2).

Kinetically inert metals to increase the transition-state energy. Transitioning from a porous MOF phase to a dense phase requires ligand exchange or geometric reorganization around the metal ions. A major component in the energy barrier for reorganization towards a dense phase is the inherent kinetics of ligand exchange of the metal ion (FIG. 2a,b). Owing to their different electronic configurations and ionic radii, transition metal ions exhibit disparate ligand-exchange kinetics, which are most often quantified by the homoleptic aquo complex self-exchange rate. The rate of ligand exchange in octahedral aquo complexes spans nearly 20 orders of magnitude from labile Cu^{2+} and Cr^{2+} at $5.9 \times 10^9\ s^{-1}$ to highly inert Ir^{3+} at $1.1 \times 10^{-10}\ s^{-1}$ (REF.[29]) (FIG. 2a). MOFs formed with kinetically inert metals can be exceptionally robust (FIG. 3a). For instance, the most widely used transition metal ion in MOF synthesis with a metal–aquo self-exchange rate slower than $1\ s^{-1}$ is Cr^{3+}, which forms carboxylate frameworks stable to H_2O, steam and even high pressures of H_2S (REFS[30–32]). Cation inertness can be a better predictor of stability than metal–ligand bond strength, as was demonstrated in the MIL-53 and MIL-47 family of isostructural frameworks, for which chemical stability decreases in the order $Cr^{3+} > Al^{3+} > V^{4+}$, which is in accordance with the H_2O substitution rates of the metal–aquo complexes but not with the thermodynamic metal–oxygen bond strengths[33]. For the M_2DOBDC (MOF-74 or CPO-27; $DOBDC^{4-}$ = dioxidobenzenedicarboxylate and M is a transition metal)[34,35] family of frameworks, partial replacement of Mg^{2+} with the more inert Ni^{2+} increases the stability towards H_2O (REF.[36]). Replacement of the native Zn^{2+} with Ni^{2+} in MOF-5 also increases the H_2O stability of the resulting Ni-MOF-5 (REF.[37]). Furthermore, in a family of MOFs formed from linear bistriazolate linkers, M_2Cl_2BBTA ($BBTA^{2-}$ = 1*H*,5*H*-benzo(1,2-d:4,5-d′) bistriazolate)[38,39] and M_2Cl_2BTDD ($BTDD^{2-}$ = bis(1*H*-1,2,3-triazolato[4,5-b],[4′,5′-i])dibenzo[1,4]dioxin)[40,41], stability towards H_2O and NH_3 decreases in the order $Ni^{2+} > Co^{2+} > Mn^{2+} > Cu^{2+}$, in agreement with the trend in metal–aquo substitution rates[42,43]. On the basis of these examples, the metal-ion–ligand substitution rate is a systematic descriptor of MOF stability that, nevertheless, is infrequently recognized in the literature.

The trend in stability for MOFs based on the ligand-exchange rate is distinct from the stability trends for divalent metal complexes observed by Irving and Williams[44,45], with the most notable divergence observed for many Cu^{2+} materials. Owing to the d^9 electronic configuration of Cu^{2+}, resulting in a Jahn–Teller distortion, its complexes exhibit short, strong bonds to four equatorial ligands, accounting for the high measured stability constants for ligand complexes. However, these complexes also exhibit extremely rapid ligand exchange

at axial positions, leading to a stability for many Cu^{2+} MOFs that is lower than that expected from the Irving–Williams series.

Stronger bonds to stabilize the porous phase relative to the transition state. The weakest link in a MOF is commonly the metal–ligand bond. Thus, the stability towards polar analytes can be augmented by increasing the heterolytic metal–ligand bond strength[46–49], which lowers the energy of the porous framework relative to the heterolytic bond-breaking transition state[50] (FIG. 2d). Increasing the donor strength of the ligand, which can be quantified by the ligand basicity (FIG. 2c), increases the heterolytic metal–ligand bond strength, particularly for late transition metals, and enhances MOF stability. For example, MOFs containing pyrazolate or imidazolate ligands in combination with late transition metals often exhibit very high chemical stability (FIG. 3b), which is due to the stronger donating ability of these ligands versus carboxylates. Ligands with greater donating ability than pyrazolates have not been widely explored in MOF chemistry, primarily owing to synthetic difficulties in either accessing the ligand or crystallizing the framework. Yet, further increasing the donating ability may not increase stability towards H_2O because of the concomitant increase in the driving force for metal–ligand bond hydrolysis.

An additional strategy for increasing the metal–ligand bond strength for carboxylate frameworks is to increase the valency of the metal ion. Although augmenting the ligand donor strength is successful for late transition metals because it results in stronger, more covalent bonds, the ionic bond strength can be increased when using carboxylate ligands by increasing the charge density on the metal ion. Higher-valent metals, such as Ti^{4+}, Zr^{4+}, Cr^{3+} and Al^{3+}, paired with carboxylates, form stronger metal–ligand bonds than those constructed with divalent metal ions.

Although often thought of as a route towards the thermodynamic stabilization of the porous phase, increasing the metal–ligand bond strength may not change the net driving force for the transition to the dense phase, because the dense phase with the same metal–ligand bonds is equally stabilized (FIG. 2d). For example, the Zn^{2+} frameworks MOF-5, with carboxylate (pK_a(dimethyl sulfoxide (DMSO)) = 11.1)[51]

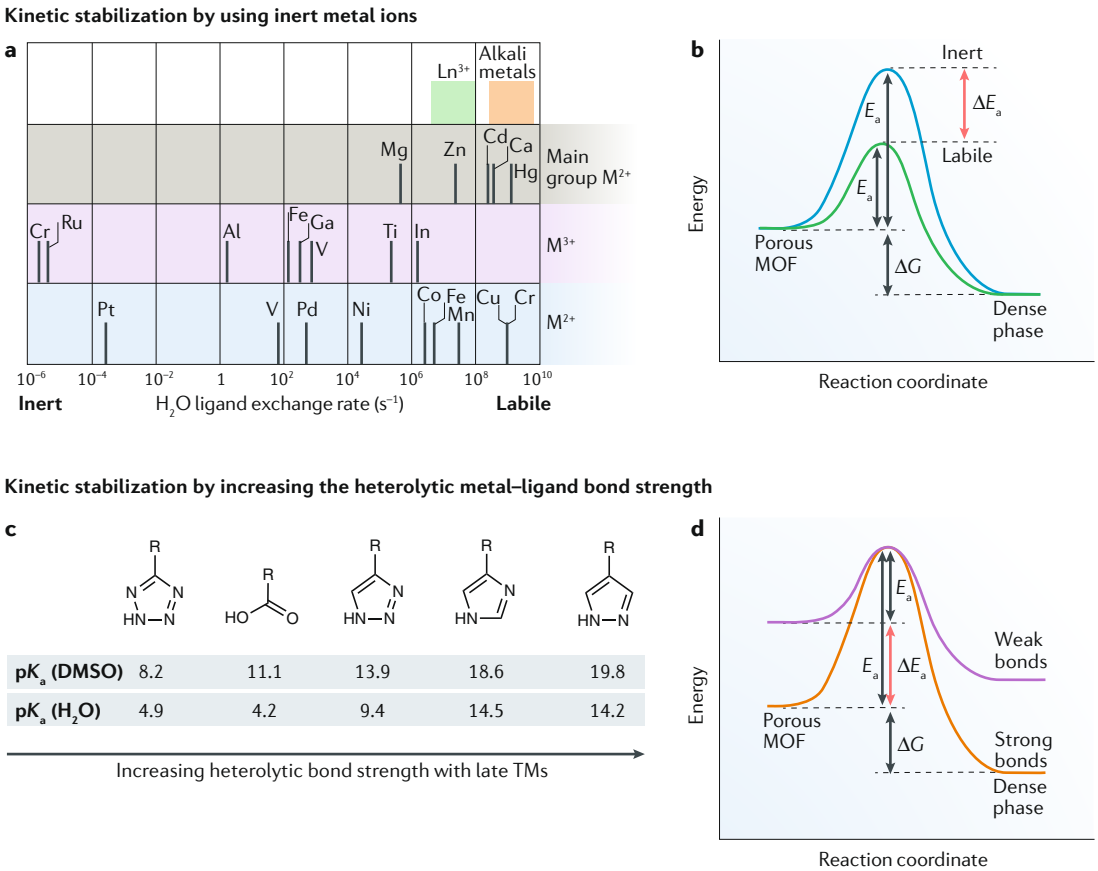

Fig. 2 | **Routes towards kinetic stabilization of MOFs.** Methods towards stabilization of the porous phase of metal–organic frameworks (MOFs) with respect to the dense phase must increase the activation energy barrier (E_a). **a** | Metal–aquo self-exchange rate constants for various metal (M) ions[29,213,214]. **b** | Increasing the inertness of the metal ion increases the activation energy barrier for rearrangement to the dense phase. **c** | The use of more strongly donating azolate ligands, as measured using pK_a values[51,52,215], in combination with late transition metals (TMs), results in stronger metal–ligand bonds. **d** | Increasing the heterolytic metal–ligand bond strength increases the activation energy barrier for a bond-breaking transition state, while not affecting the net driving force for the transition towards the dense phase. ΔG, change in the Gibbs free energy; DMSO, dimethyl sulfoxide; Ln, lanthanide.

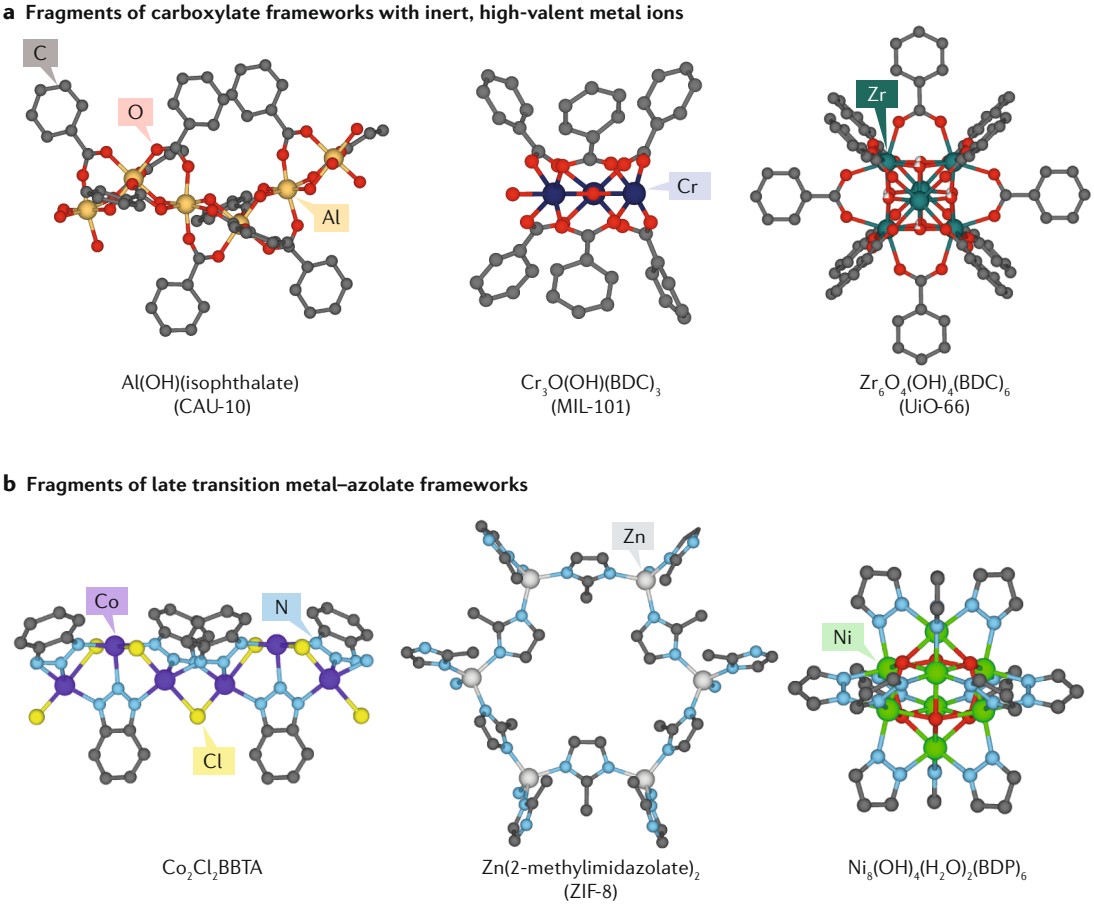

Fig. 3 | **MOF building blocks with high kinetic stability.** Examples of metal–organic framework (MOF) building blocks with high kinetic stability include those based on carboxylate frameworks containing inert, high-valent metal ions[30,54,109] (panel **a**) and late transition metal–azolate frameworks[38,118,216] (panel **b**). H atoms omitted for clarity. $BBTA^{2-}$, 1*H*,5*H*-benzo(1,2-d:4,5-d′) bistriazolate; BDC^{2-}, 1,4-benzenedicarboxylate; BDP^{2-}, 1,4-benzene dipyrazolate; ZIF, zeolitic imidazolate framework.

ligands, and Zn-methylimidazolate (ZIF-8; imidazolate pK_a(DMSO) = 18.6)[52] have nearly identical energy penalties for the porous phase with respect to the corresponding dense phases[17]. Nonetheless, the increased metal–ligand bond strength in ZIF-8 results in greater kinetic stability relative to MOF-5, especially towards coordinating species, owing to an increased energy barrier for heterolytic metal–ligand bond breaking[50].

Linker and node connectivity. The activation energy barrier can also be increased by increasing the connectivity of the framework components, which enhances the stability in a manner similar to the chelate effect. This stabilization results from the increase in the number of metal–ligand bonds that must dissociate or rearrange simultaneously for a phase transition to occur or a pore to collapse. For instance, the barrier to linker removal or reorganization is greater for a tetratopic carboxylate, such as the linker of $Zr_6O_4(OH)_4(HCOO)_4(TBAPy)_2$ (NU-1000; $TBAPy^{4-}$ = pyrene tetra-*p*-benzoate)[53], than a ditopic carboxylate, such as the biphenyl dicarboxylate ($BPDC^{2-}$) linker of $(Zr_6O_4(OH)_4(BPDC)_6$ (UiO-67)[54]. Similarly, frameworks composed of secondary building units (SBUs) (that is, the metal–oxo–hydroxo clusters of the framework) with greater connectivity exhibit enhanced stability; this is exemplified by MOFs constructed from Zr^{4+} oxo–hydroxo nodes, which can be linked by 6, 8, 10 or 12 carboxylate groups, with the stability generally increasing with node connectivity[55–57].

Sterics and hydrophobicity. Steric shielding of metal–ligand bonds can impede the access of H_2O and other coordinating vapours to these delicate linkages[57–61]. However, this strategy may also decrease the overall porosity as well as inhibit the access of desirable sorbates to the framework sites, which often exhibit the strongest guest-binding interactions.

Stability effects of gases and vapours

Coordinating gases and vapours

Exposure to coordinating gases and vapours, such as H_2O, NH_3 and H_2S, can perturb the bonding and connectivity of a MOF, frequently resulting in a decrease in the useful surface area and porosity. The ability of a MOF to withstand exposure is directly related to the energy barrier towards ligand rearrangement or substitution. Several reaction pathways can be operative, including ligand substitution[50], metal–ligand bond hydrolysis[62–64], coordination-induced ligand rearrangement[65,66] or pore collapse owing to capillary forces[67,68].

Common to all mechanisms is a requirement for ligand rearrangement around the SBU, as well as some degree of heterolytic metal–ligand bond breaking. These factors directly relate the stability of a MOF towards coordinating gases and vapours to the kinetics of ligand exchange at the metal centre and the heterolytic metal–ligand bond strength. For example, theoretical calculations for metal–ligand hydrolysis and H_2O substitution reactions reveal that hydrolysis to form the metal hydroxide and the protonated ligand is universally downhill for diverse frameworks, including Zn-MOF-5, Cu-HKUST-1, Cr-MIL-101 and Zn-ZIF-8. However, the activation energy barrier for ligand substitution is much larger for Cr-MIL-101 and Zn-ZIF-8, which is in accordance with the experimentally observed high steam stability for these two frameworks compared with Zn-MOF-5 and Cu-HKUST-1 (REF.[50]).

The stability trends of MOFs towards polar gases are largely dependent on the acidity and nucleophilicity of the gas. The stability of MOFs towards NH_3 and H_2S follow the same trend as that for H_2O. However, the greater nucleophilicity of NH_3 makes ligand substitution potentially more favourable. NH_3 reacts with H_2O to form NH_4OH, which is highly corrosive and may result in metal–ligand bond hydrolysis[69]. For the more acidic H_2S, which has a pK_a of 7.0 in H_2O and is, thus, seven orders of magnitude more acidic than H_2O, protonation of the ligand occurs more readily, affording a metal sulfhydryl or sulfide[32]. Furthermore, H_2S is highly nucleophilic and coordinates strongly to metal ions; therefore, H_2S can readily substitute for a framework ligand.

Acidic and oxidizing gases and vapours

Designing materials that are stable to acidic and oxidizing gases such as SO_2, NO_x and halogens (X_2) presents unique challenges. In particular, oxidation of the metal centres by an oxidizing gas can drastically alter the kinetics of ligand substitution and the preferred ligand geometry around the metal centre. Moreover, many materials are stable to corrosive gases in single-component studies, but in the presence of humid air, various new challenges arise from potential side reactions that form strong acids[70]. For example, in combination with H_2O vapour, SO_2 forms sulfurous acid (H_2SO_3), and over time in the presence of O_2, SO_2 can form SO_3 and sulfuric acid (H_2SO_4)[71]. Consequently, SO_2 adsorption in humid air, which is relevant for industrial applications, is problematic, and linker protonation resulting in the formation of metal sulfites or sulfates can be extremely destructive[72].

The capture of NO_x presents additional challenges. Much the same as SO_2, both NO and NO_2 under humid oxidizing conditions can form strong acids (HNO_2 and HNO_3), which may protonate linkers to cause framework degradation. NO and NO_2 can also undergo various redox reactions, such as NO disproportionation ($3NO \rightarrow NO_2 + N_2O$), NO oxidation ($2NO + O_2 \rightarrow 2NO_2$) or NO_2 dimerization followed by disproportionation ($2NO_2 \rightarrow N_2O_4 \rightarrow NO^+ + NO_3^-$)[73].

NO^+ is a particularly destructive species that reacts with aromatics, amino groups and transition metals, causing irreversible framework damage. Therefore, in the development of frameworks for NO_x capture, it is necessary to either employ methods to mitigate the reactive chemistry of NO_x or to design materials that accommodate the daughter products[74].

Framework design for gas capture

The modularity of MOFs allows for three main strategies to increase the interaction strength between the framework and polar gases. The first approach relies on MOFs containing metal ions with open coordination sites, typified by frameworks such as HKUST-1, MOF-74 and M_2Cl_2BBTA. These frameworks can exhibit strong affinities for Lewis basic gases and oxidizing gases. However, direct coordination by an analyte gas to a framework node can lead to ligand rearrangement or hydrolysis of the metal–ligand bond. Therefore, the deployment of this method requires robust framework stability. The second strategy focuses on the installation of functional groups, such as NH_2, OH or SO_3H, on the organic ligands to modulate the framework polarity and hydrophilicity. However, the functional groups occupy pore volume and decrease the surface area of the resulting frameworks. Thirdly, auxiliary ligands integral to the SBUs can be leveraged as strongly interacting sites for polar gases. For instance, the μ-OH moieties in $Zr_6O_4(OH)_4^{12+}$ SBUs serve as primary sorption sites for H_2O and SO_2 (REFS[55,75]). Note that, although augmenting the surface area may increase the overall capacity for gas uptake at high relative pressure, it does not increase the affinity for polar gases at low relative pressure. Increasing the surface area increases the number of purely dispersive interaction sites, but these weak binding sites are insufficient for selective polar gas capture.

H_2O

Occurrence and applications

The stability of MOFs towards liquid H_2O and H_2O vapour, which can be distinct, have been extensively investigated[55–57,76] because H_2O is the most common coordinating and corrosive gas present in the atmosphere, as well as in many applications, such as post-combustion gas streams[6,77], gas sensing[78] or fuel cells containing proton-conducting materials[79]. Additionally, the capture of H_2O vapour has several desirable applications, including dehumidification[67,80,81], heat transfer[82,83] and atmospheric H_2O capture[41,84–88]. These applications rely on cycles in which H_2O alternatingly fills the pores and is then desorbed, necessitating extensive cycling stability. When compared with state-of-the-art zeotypes, which exhibit capacities near 0.3 g g^{-1}, MOFs can exhibit much higher gravimetric (gram of H_2O per gram of sorbent) capacities, although the difference is slightly smaller when the volumetric capacity (cm^3 H_2O per cm^3 sorbent) is used (FIG. 4; TABLE 1). H_2O is unique among the gases and vapours considered herein because it is a liquid at standard temperature and pressure (STP) and thus completely fills the pore interior of a porous material above a specific humidity. Strategies for the design of H_2O sorbents have focused on optimizing the relative humidity (RH) of pore filling, such that it is favourable under the temperature and vapour pressure conditions of a given application. The partial pressure of pore filling is highly dependent on the pore size and hydrophilicity.

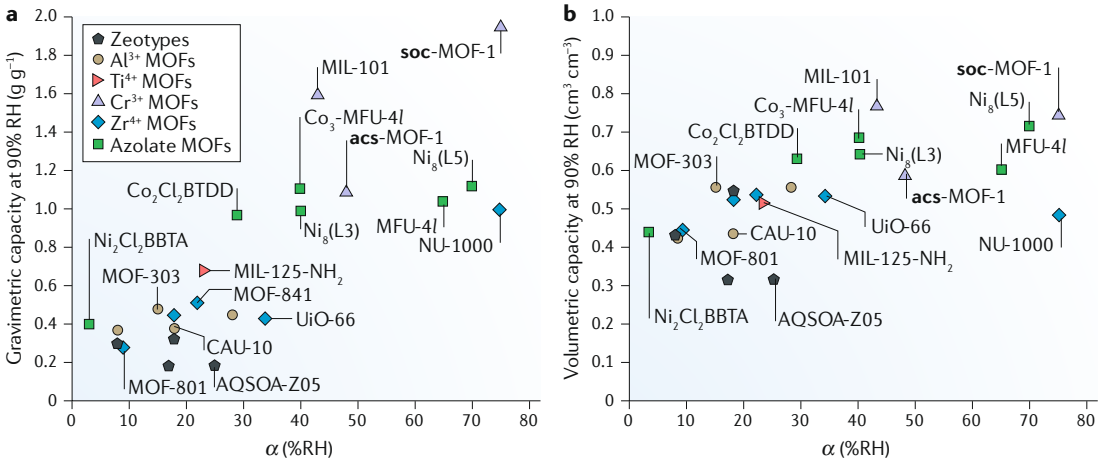

Fig. 4 | **H_2O capacities of porous solids. a** | Gravimetric uptake capacity versus α, the relative humidity (RH) value at which half the total capacity is reached. Materials with larger pores can achieve higher gravimetric capacities, with a concomitant reduction in hydrophilicity, than those with small pores. **b** | Plotting the capacity in volumetric units highlights the reduced variation in total capacity as a function of hydrophilicity. Data and references are listed in TABLE 1. $BBTA^{2-}$, 1*H*,5*H*-benzo(1,2-d:4,5-d′)bistriazolate; $BTDD^{2-}$, bis(1*H*-1,2,3-triazolato[4,5-b],[4′,5′-i])dibenzo[1,4]dioxin; MOF, metal–organic framework.

Small pores fill at lower RH than do large pores, which fill closer to 100% RH[55,76,89]. Framework hydrophilicity can be modulated by appending polar groups to the organic ligands. However, this strategy reduces the total pore volume and leads to the H_2O uptake step broadening over a larger RH range, both of which lower the usable capacity[48,90–92]. Anion and cation exchange strategies at the node can be used to control the partial pressure of pore filling without modifying pore size and shape, but require consideration of the changes to framework stability inherent to SBU alterations[93,94].

MOF sorbents for H_2O

H_2O sorbents with extended cycling stability generally fall into two categories: those with high-valent, inert, early transition metal–carboxylate frameworks, and those with late transition metal–azolate frameworks. The stability of MOFs towards H_2O has been reviewed previously[57,76] and a comprehensive review of MOFs investigated for H_2O sorption is available[83]. Here, we focus on the trends in stability for MOF building blocks and the high-performance sorbents constructed from kinetically stable building blocks. The H_2O capacities of H_2O-sorbing porous materials that have achieved the highest uptake in a specific region of RH are summarized in TABLE 1 and compared in FIG. 4.

Inert, high-valent metal carboxylates. Zr^{4+} MOFs that feature $Zr_6O_4(OH)_4(RCOO)_{12}$ nodes, typified by the terephthalate-linked UiO-66 (REF. [54]), have been widely explored as stable H_2O sorbents[95]. By varying the ditopic carboxylate linker from the smallest (fumarate, MOF-801)[96] to the largest (4,4′-[(2,5-dimethoxy-1,4-phenylene) bis(ethyne-2,1-diyl)]dibenzoic acid, PIZOF-2)[97], the pore size can be modified from 6 Å to 20 Å, enabling the H_2O pore-filling step to be tuned from 9% RH to 75% RH[55]. Although Zr^{4+} carboxylate frameworks are generally thought of as stable to H_2O, this is not the case for all members of the family: MOF-805, MOF-806 and MOF-808 undergo notable degradation upon H_2O sorption, whereas MOF-801, MOF-802, MOF-841 and UiO-66 are stable to at least five cycles of H_2O uptake and release[55]. Differences in the stability of hexanuclear zirconium frameworks are often attributed to the connectivity of the nodes and the rich defect chemistry of zirconium MOFs[68,98–101], with more defective frameworks collapsing faster, owing to their lower connectivity. Recently, $Zr_6O_4(OH)_4(HCOO)_4$(methylene diisophthalate)$_2$ (MIP-200) was reported to have a H_2O capacity of nearly 40 wt%, which was achieved below 25% RH; moreover, the framework exhibits exceptional chemical and H_2O cycling stability over 50 cycles, attributed to residual framework anions bound to the nodes. MIP-200 withstands NH_4OH vapour, 6 M H_3PO_4, aqua regia, HNO_3 and HCl at reflux[102].

Another family of exceptionally stable carboxylate MOFs is based on nodes consisting of inert Al^{3+} ions linked by carboxylates, forming the oxo-centred trinuclear SBUs found in $Al_3O(OH)(BTC)_2$ (Al-MIL-100)[103,104], or infinite chains of Al^{3+} bridged by OH groups, an SBU found in Al(OH)(BDC) (Al-MIL-53)[105]. Al(OH)(fumarate), which is isoreticular to MIL-53, is a mass-produced MOF that has been tested as a coating on a full-scale heat exchanger for heat-transfer processes. This MOF coating exhibited 95% capacity retention for H_2O after 360 cycles[106]. Aluminium MOFs formed with bent dicarboxylate linkers, typified by Al(OH)(isophthalate) (CAU-10)[107–109], exhibit exceptional H_2O sorption characteristics for heat-transfer processes. The synthesis of CAU-10 can be readily scaled[110] and the material has an H_2O isotherm step well positioned for use in adsorptive heat-transfer processes. A heat exchanger coated with a sample of CAU-10 in a binder exhibited negligible loss in H_2O capacity after 10,000 cycles[107]. Replacing the isophthalate linker in CAU-10 with the 2,5-furandicarboxylate linker produces the isostructural MIL-160 framework[111], which has an increased H_2O affinity and a similar gravimetric H_2O capacity. Furthermore, the

recently reported Al-MOF-303 uses 2,5-pyrazole dicarboxylate as the linker and retains its H_2O capacity of 33 wt% after 150 cycles[88].

Of the first-row transition metals, Cr^{3+} is the most kinetically inert and forms exceptionally robust frameworks with multitopic carboxylates. Cr^{3+} frequently forms SBUs similar to those formed by Al^{3+}. For instance, $Cr_3O(OH)(BTC)_2$ (Cr-MIL-100) and Cr-MIL-101 (REF.[30]) comprise trinuclear oxo-centred clusters, and Cr(OH)(BDC) (Cr-MIL-53)[31] consists of infinite chains of metal ions bridged by OH groups. Cr-MIL-101 has been widely explored for H_2O sorption, owing to its exceptional overall H_2O uptake of 1.6 g g^{-1}, as well as its high cycling stability[91,112–114]. As a consequence of its exceptional inertness, the synthesis of Cr^{3+} frameworks is challenging, owing to the irreversibility of bond formation on a reasonable timescale. To obtain H_2O sorbents with both high capacity and stability, one strategy to overcome the difficulties of direct Cr^{3+} MOF synthesis is to first crystallize an Fe^{3+} carboxylate framework and subsequently exchange Fe^{3+} for Cr^{2+} to incorporate chromium into the framework. A labile Cr^{2+} ion can rapidly enter the SBU and, once inserted, it is oxidized by Fe^{3+} to Cr^{3+}, which is, thereby, kinetically trapped.

Table 1 | **H_2O capacities for selected porous materials**

Porous material	α[a] (%RH)	Capacity at 95% RH (g g^{-1})	Crystal density (g cm^{-3})	Uptake (cm^3 cm^{-3})	Refs
Co_2Cl_2BTDD	29	0.97	0.65	0.6305	41
Cr-**soc**-MOF	75	1.95	0.381	0.74295	67
Cr-MIL-101	43	1.6	0.48	0.768	91
MOF-841	22	0.51	1.05	0.5355	55
MOF-801	9	0.28	1.59	0.4452	55
Ni_2Cl_2BBTA	3	0.4	1.1	0.44	43
Cr-**acs**-MOF	48	1.09	0.539	0.58751	116
CAU-10	18	0.38	1.15	0.437	107
MIL-160	8	0.37	1.15	0.4255	111
MOF-303	15	0.48	1.159	0.55632	88
Ti-MIL-125-NH_2	23	0.68	0.757	0.51476	117
Al-fumarate	28	0.45	1.24	0.558	83
MIP-200	18	0.45	1.16	0.522	102
UiO-66	34	0.43	1.24	0.5332	83
Ni_8(L3)	40	0.99	0.69	0.6831	120
Ni_8(L5)	70	1.12	0.64	0.7168	120
Zn-MFU-4*l*	65	1.04	0.58	0.6032	93
Zn_2Co_3-MFU-4*l*	40	1.11	0.58	0.6438	93
NU-1000	75	1	0.486	0.486	83
ALPO-78	18	0.32	1.7	0.544	216
AQSOA Z02	8	0.3	1.43	0.429	83
AQSOA Z01	17	0.18	1.75	0.315	83
AQSOA Z05	25	0.18	1.75	0.315	83

BBTA^{2-}, 1*H*,5*H*-benzo(1,2-d),(4,5-d′)bistriazolate; BTDD^{2-}, bis(1*H*-1,2,3-triazolato[4,5-b],[4′,5′-i]) dibenzo[1,4]dioxin; L, ligand; MOF, metal–organic framework. [a]α is the % relative humidity (RH) at which half of the total uptake is reached.

This strategy was pursued to synthesize the record-setting Cr-**soc**-MOF[67,115], which has a H_2O uptake of nearly 2 g g^{-1}, and Cr-**acs**-MOF (NU-1500)[116]. Testament to the analysis of stability based on the metal–aquo exchange rate presented above, the Fe^{3+} analogues and the Al^{3+} analogue for the mesoporous **soc**-MOF collapse, owing to capillary forces during pore filling or to desorption of H_2O from the pores during activation, whereas the Cr^{3+} derivatives withstand repeated H_2O cycling[67,116].

Carboxylate frameworks that incorporate other metal ions, including Ti^{4+} and Fe^{3+}, have also been investigated for H_2O-sorption applications. $Ti_8O_8(OH)_4(H_2N\text{-}BDC)_6$ (Ti-MIL-125-NH_2) absorbs more than 50 wt% H_2O below 25% RH with minimal loss of capacity over 10 cycles[117]. Additionally, $Fe_3O(OH)(BTC)_2$ (Fe-MIL-100) was investigated for latent cooling load reduction and a MOF coating on a heat exchanger could be cycled 2,000 times while losing only 4.5% of the original capacity[80]. Carboxylate MOFs that use late transition metals or those with a lower valency than that of Fe^{3+} are not candidates for H_2O-sorption applications, owing to stability concerns.

Late transition metal–azolate frameworks. Moving from hard, weakly donating carboxylate ligands to the comparatively soft, strongly donating azolate ligands, such as triazolate, pyrazolate and imidazolate, engenders heterolytically stronger metal–ligand bonds with late transition metals. This strategy has been effective in creating robust Zn^{2+} MOFs with imidazolates and pyrazolates, even though Zn^{2+} is quite labile. ZIFs have been widely explored as H_2O sorbents and exhibit exceptional stability, yet their general hydrophobicity and limited total pore volume restricts the use of ZIFs in applications such as heat transfer and H_2O harvesting[83,112]. Pyrazolate frameworks have been explored as H_2O sorbents for heat transfer; however, the topologies heretofore synthesized with these linkers lack open coordination sites and the frameworks are typically hydrophobic. MOFs composed of linear bispyrazolate[118] or square tetrapyrazolate[119] linkers with $Ni_8(OH)_4(H_2O)_2$ SBUs can exhibit exceptional stability and are also highly hydrophobic, absorbing H_2O only above 80% RH in one case[120]. The hydrophilicity of pyrazolate frameworks can be modulated by modifying the organic linkers, although these modifications can reduce the overall H_2O capacity and broaden the H_2O uptake step[48].

MOFs constructed from linear bistriazolate frameworks contain a high density of open coordination sites, making them very hydrophilic. M_2Cl_2BTDD has a topology similar to that of MOF-74, including hexagonal pores lined with infinite 1D chains of metal ions that exhibit open coordination sites, and the Co^{2+} and Ni^{2+} analogues are stable to repeated H_2O uptake[41]. Although the size of its mesopores exceed the critical diameter for H_2O capillary condensation (the diameter above which hysteresis should be observed), Co_2Cl_2BTDD reversibly sorbs H_2O without hysteresis, owing to H_2O coordination at the open metal sites prior to the pore-filling step, which reduces the effective pore diameter below the critical diameter. M_2Cl_2BBTA is an analogue of M_2Cl_2BTDD with smaller pores and is, thus, much more

hydrophilic, capturing H_2O near 0% RH[43]. Among the metal ions tested, Ni_2Cl_2BBTA is the most stable, with the stability trend in line with the metal–aquo substitution rates. Although they form hexagonal structures with the majority of late transition metals, linear bis-triazolate linkers form a cubic structure when treated with Zn^{2+}. The resulting framework, $Zn_5Cl_4(BTDD)_3$ (MFU-4*l*)[121,122], has a large H_2O uptake capacity of >1 g g^{-1}. Cation exchange of the native Zn^{2+} for Co^{2+} enables the RH of H_2O uptake to be varied over a range of nearly 30% without decreasing the overall capacity, owing to the greater propensity for a tetrahedral Co^{2+} to accept a fifth ligand[93]. However, the cubic, BTDD-based frameworks exhibit decreased stability relative to the hexagonal frameworks, with the fully exchanged Co^{2+} material collapsing in the presence of H_2O vapour[93].

NH_3

Occurrence and applications

NH_3 is an industrial gas produced on a massive scale and its toxicity has prompted considerable research focused on its detection and sensing[78,123,124], as well as the development of personal protective equipment (PPE)[125–128]. To lower the NH_3 concentration below the US National Institute for Occupational Safety and Health's immediate danger threshold (300 ppm)[129] or below the odour threshold of 5 ppm (REF.[130]), sorbents must have a high affinity and capacity for NH_3 at low relative pressure. As a reference, the benchmark sorbent zeolite 13X has a moderate capacity of 9 mmol NH_3 per g of material at STP[131]. Research in materials for PPE has not focused substantially on framework stability because single-use sorbents that collapse on contact with NH_3 are acceptable under certain conditions. However, stability remains important, as pore collapse during use can affect the performance of a protective sorbent. Other applications may require extensive NH_3 cycling stability. For instance, NH_3 is a common impurity in feed gas streams and can poison catalysts and membranes, necessitating the use of sorbents to capture NH_3 prior to the desired chemical process. Finally, on a thermodynamic basis, NH_3 is an excellent working fluid for heat transfer in adsorption heat pumps, which require many thousands of adsorption cycles and materials with extreme stability to this corrosive gas[83].

Table 2 | **Static NH_3 capacities for selected materials**

Porous material	NH_3 capacity (mmol g^{-1})	Refs
Zeolite 13X	9	131
Amberlyst 15	11	131
MCM-41	7.9	131
UiO-66-NH_2	9.84	40
HKUST-1	12.1	132
DUT-6	12	139
DUT-6-$(OH)_2$	16.4	139
Fe-MIL-101-SO_3H	17.8	144
Al-MFM-300	13.9	131
P1-PO_3H_2	18.7	147
P2-CO_2H	16.1	147
Mn_2Cl_2BTDD	15.47	40
Co_2Cl_2BTDD	12	40
Ni_2Cl_2BTDD	12.02	40
Cu_2Cl_2BTDD	16.74	42
Co_2Cl_2BBTA	17.95	42
Ni_2Cl_2BBTA	14.68	42
Cu_2Cl_2BBTA	19.79	42
Al-MFM-300	13.9[a]	131
Prussian blue	12.5	145
CoHCC	21.9	145
CuHCF	20.2	145
$MgCl_2$	54.8	217

Materials tested at 1 bar NH_3 and 298 K. $BBTA^{2-}$, 1*H*,5*H*-benzo(1,2-d:4,5-d′)bistriazolate; $BTDD^{2-}$, bis(1*H*-1,2,3-triazolato[4,5-b],[4′,5′-i])dibenzo[1,4]dioxin; HCC^{3-}, hexacyanocobaltate; HCF^{3-}, hexacyanoferrate. [a]Measured at 293 K.

MOF sorbents for NH_3

The static and breakthrough NH_3 capacities of selected porous materials are summarized in TABLE 2 and TABLE 3, respectively, and compared in FIG. 5.

Lewis acidic open metal sites. To capture NH_3 at low relative pressure, one common strategy is the use of MOFs with Lewis acidic open metal sites, including HKUST-1, MOF-74 and M_2Cl_2BBTA frameworks. For example, HKUST-1 exhibits a high capacity for NH_3 of 12.1 mmol NH_3 g^{-1} MOF at 1 bar (REF.[132]) but loses crystallinity upon NH_3 exposure in under 2 h[133]. On the basis of NMR data, the reaction of HKUST-1 with anhydrous NH_3 produces a diamine copper complex with a pendant anionic trimesate ligand, whereas in the presence of H_2O, the reaction yields $Cu(OH)_2$ and $(NH_4)_3BTC$[69]. A polyvinylidene difluoride coating was found to protect HKUST-1 from NH_3; the composite maintained crystallinity and a constant NH_3 capacity over 28 days[134]. On the basis of dynamic measurements, which determine the capacity of a material prior to 'breakthrough', analogues of MOF-74 have high capacities for NH_3, with the champion Mg^{2+} material able to capture 7.6 mmol g^{-1} before breakthrough, although the presence of H_2O substantially decreased the uptake[135]. By contrast, Cu-MOF-74 can adsorb more NH_3 with H_2O vapour present, although the material was unstable to NH_3 (REF.[136]).

By using strong donor triazolate linkers, M_2Cl_2BTDD materials were the first examples of MOFs to exhibit a high density of open metal sites that are stable to repeated sorption and desorption of NH_3 (REF.[40]). The Ni^{2+} analogue is stable to complete pore filling with NH_3, which occurs in a stepwise process near 0.8 bar of pure NH_3 at 263 K (REF.[42]). Owing to their greater density of open coordination sites, the smaller-pore M_2Cl_2BBTA materials capture substantially more NH_3, particularly at low pressures, than their larger-pore analogues. The Cu^{2+} analogue has the largest static capacity at 1 bar and 298 K of any MOF, but it is unstable to even low concentrations of NH_3, which compromises its dynamic breakthrough performance. Co_2Cl_2BBTA loses crystallinity at 1 bar of NH_3 but is stable to 1 mbar NH_3,

Table 3 | **Breakthrough NH_3 capacities for selected materials**

Porous material	NH_3 concentration (ppm)	NH_3 capacity (mmol g^{-1})		Refs
		Dry conditions	Humid (80% RH) conditions	
UiO-66-OH	2,880	5.69	2.77	140
Zeolite 13X	1,440	2.86	0.62	135
P1-PO_3H_2	2,880	5.2	7.2	147
P2-CO_2H	2,880	6.7	7.4	147
HKUST-1	1,000	6.76	10.12	218
Mg-MOF-74	1,440	7.6	1.7	135
Co_2Cl_2BTDD	1,000	4.75	3.37	42
Co_2Cl_2BBTA	1,000	8.53	4.34	42
Cu_2Cl_2BTDD	1,000	7.52	5.73	42

Materials tested at 298 K. $BBTA^{2-}$, 1*H*,5*H*-benzo(1,2-d:4,5-d′)bistriazolate; $BTDD^{2-}$, bis(1*H*-1,2,3-triazolato[4,5-b],[4′,5′-i])dibenzo[1,4]dioxin; MOF, metal–organic framework; RH, relative humidity.

the conditions of a typical breakthrough test. This stability enables Co_2Cl_2BBTA to capture the greatest quantity of NH_3 of any material under dry breakthrough conditions. The Ni^{2+} material is the most stable among the BBTA frameworks, and the stability trend based on the NH_3 pressure required to effect a loss of crystallinity and porosity in this family of triazolate MOFs is consistent with expectations based on the substitution kinetics of the metal–hexaaquo complexes[42].

Ligand functionalization. MOFs without open coordination sites have also been investigated for NH_3 capture. In this case, the affinity for NH_3 is typically increased through ligand functionalization with polar or acidic groups. For example, NH_2-functionalized MOF-5 has a high capacity for NH_3, sorbing 6.2 mmol g^{-1} in breakthrough testing in a stream of 1% NH_3, which exceeds the capacity of Zn-MOF-74 (REF.[137]). Compared with the parent materials, composites of graphene oxide with MOF-5 show increased NH_3 uptake, although the frameworks collapse rapidly in the presence of NH_3 (REF.[138]). Zn^{2+} frameworks isoreticular to MOF-5 and featuring ligands with free OH groups can capture up to 16.4 mmol g^{-1} in static equilibrium measurements at STP, albeit with loss of surface area and crystallinity[139].

For the Zr^{4+} carboxylate framework UiO-66, diverse organic functional groups have been explored to enhance the affinity for NH_3 (REF.[84]). NH_2-functionalized UiO-66 (UiO-66-NH_2) outperforms derivatives with more acidic but bulkier functional groups, such as –COOH and –SO_3H, in breakthrough measurements, presumably owing to pore-clogging effects with larger moieties[140]. Similarly, the addition of Cu^{2+} to pendant free carboxylate groups can enhance equilibrium NH_3 uptake, albeit at the expense of the rate of gas diffusion[141]. Further investigation of UiO-66-NH_2 revealed that a fraction of the NH_2 groups are protonated, forming –NH_3Cl under typical acidic synthesis conditions, which may increase affinity for NH_3. Additionally, reaction of the NH_2 groups with acetaldehyde to afford the hemiaminal or aziridine products enhances the NH_3 capacity[142]. Although stable to short exposure times[133], repeated cycling of NH_3 uptake in UiO-66-NH_2 leads to a loss of capacity, surface area and crystallinity[40].

Other materials. Trivalent Cr^{3+}, Al^{3+} and Fe^{3+} carboxylate MOFs can exhibit increased stability towards NH_3 (REF.[133]) but have not been widely explored as sorbents. A framework comprised of Al^{3+} and a biphenyl tetracarboxylate linker, termed Al-MFM-300, was stable for 50 cycles of NH_3 uptake with a high static capacity of 13.9 mmol g^{-1} at 1 bar (REF.[131]). Additionally, a highly stable Al^{3+} porphyrin MOF can be soaked in HCl or formic acid solutions to achieve up to 7.9 wt% breakthrough capacity[143]. Upon functionalization of Fe^{3+}-MIL-101 with sulfonic acid groups, it captures 17.8 mmol g^{-1} at STP and has a high affinity for NH_3 at low pressure[144].

Other families of porous materials have recently been investigated for NH_3 capture. All-inorganic Prussian blue analogues, by virtue of their high density of Lewis acidic metal sites, have particularly high static capacities for NH_3 of >20 mmol g^{-1} and can be recycled[145]. In addition, covalent organic frameworks (COFs) with robust linkages may find utility in NH_3 sorption. Although boronate ester-linked COF-10 captures 15 mmol g^{-1} at STP, slow degradation was observed with cycling, as the linkages are susceptible to nucleophilic attack[146]. By contrast, porous polymers with all-carbon backbones such as diamondoid structures densely functionalized with acidic groups can exhibit superlative capacity and stability for NH_3, with an uptake of 18.7 mmol g^{-1} at STP for the phosphonic-acid-functionalized material; however, diffusion is compromised, owing to the interpenetrated nature of the frameworks[144,147].

H_2S

Occurrence

H_2S is a major contaminant in flue gas streams and in many sources of natural gas, termed sour gas. When present in process streams, H_2S poisons catalysts, corrodes components and, if not removed, combusts into SO_x, a major air pollutant. Additionally, H_2S is highly toxic and heavier than air, and thus it is vital to maintain a concentration below the US Occupational Safety and Health Administration's exposure limit of 10 ppm or the odour threshold of 1.5 ppm (REFS[130]). The detection[148–150] and removal of H_2S is therefore of great interest, but limited research in the MOF community has focused on these applications.

MOF sorbents for H_2S

MOFs with open metal sites have been explored to capture H_2S, including HKUST-1, which exhibits a high capacity of 8 wt%, although, as with NH_3, the framework is unstable to H_2S. Partial protonation of the trimesate ligand by H_2S is proposed to result in framework collapse, although the formation of CuS may also drive decomposition in this case. Similar to their performance with NH_3, HKUST-1 composites with graphene oxide capture more H_2S than the parent materials but also suffer from stability issues[151,152]. The use of non-structural metal ions with open coordination sites within the metallolinkers can provide strong binding sites for H_2S

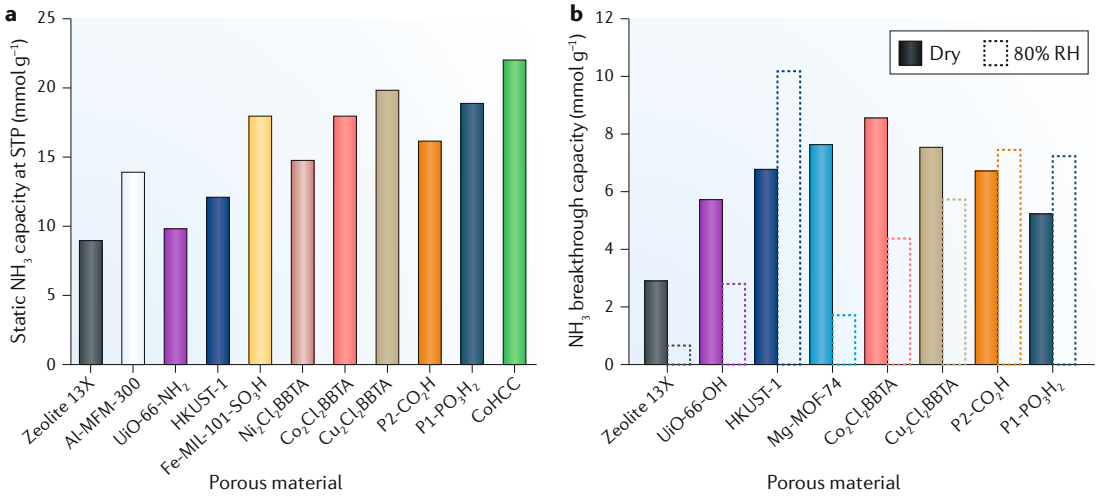

Fig. 5 | **NH_3 capacities of porous solids. a** | Static NH_3 capacity at 1 bar and 298 K (with the exception of Al-MFM-300, which was tested at 293 K) based on equilibrium isotherm data. **b** | NH_3 capacity under dynamic breakthrough conditions at 298 K in both dry and humid conditions. Materials were tested at NH_3 concentrations of 1,000 ppm (HKUST-1, Co_2Cl_2BBTA and Cu_2Cl_2BBTA), 1,440 ppm (zeolite 13X and Mg-MOF-74) or 2,880 ppm (UiO-66-OH, P2-CO_2H and P1-PO_3H_2). Data and references are listed in TABLE 2 and TABLE 3 for static and breakthrough NH_3 capacities, respectively. $BBTA^{2-}$, 1*H*,5*H*-benzo(1,2-d),(4,5-d′)bistriazolate; MOF, metal–organic framework; RH, relative humidity; STP, standard temperature and pressure.

while also maintaining framework stability. For example, UiO-67-bipyridine grafted with Cu^{2+} has a high capacity for H_2S of up to 7.8 wt%, on par with the comparatively unstable HKUST-1 (REF.[153]).

High-valent metal terephthalates, including Zr-UiO-66, Cr-MIL-101 and Ti-MIL-125, as well as their NH_2-functionalized derivatives, have been investigated for H_2S capture from natural gas[154]. The NH_2-functionalized derivatives had the highest capacities and Ti-MIL-125-NH_2 was the top performer. Each of these materials preferentially adsorbs H_2S over CO_2, although the addition of CO_2 decreases capacities for H_2S. However, the performance of Cr-MIL-101 for H_2S adsorption was superior in the presence of CO_2 (REF.[154]). Additionally, V-MIL-47 and Cr-MIL-53 have been investigated for H_2S capture at high pressures. Both of these materials appear to be stable up to 18 bar H_2S (REF.[32]), whereas Fe-MIL-53 decomposes under similar conditions, likely to iron sulfide and H_2BDC[152].

Select pyridinic MOFs with moderately inert divalent metal ions can withstand H_2S exposure. For example, $Mg_3(OH)_2$(2,4-pyridine dicarboxylate)$_2$ (Mg-CUK-1) captures >3 mmol H_2S g^{-1} MOF when exposed to 15% H_2S in N_2 and remains stable over five cycles[155]. Moreover, Ni^{2+}-pyrazine (py) frameworks that contain anionic inorganic pillars absorb both CO_2 and H_2S from natural gas streams[156] and have been investigated for H_2S separations using mixed-matrix membranes. Ni(py)$NbOF_5$ and Ni(py)AlF_5 (REF.[157]) greatly increase both the selectivity and the permeability of the host polymer membrane for H_2S, and both materials remain stable, as determined by powder X-ray diffraction, after exposure to 14 bar H_2S (REF.[158]). These Ni^{2+} materials are more stable to H_2S and H_2O than analogous Cu^{2+} frameworks comprising SiF_6^{2-} pillars, with Ni(py)AlF_5 stable to 15 cycles of H_2O uptake[159,160].

MOFs based on azolate ligands have not been widely explored for H_2S capture. Notwithstanding, Zn(tetrazolate) (**kag**-MOF-1), which is stable to H_2O and low concentrations of H_2S, selectively absorbs H_2S over long-chain hydrocarbons, owing to its small pore diameter[161].

SO_2

The static and breakthrough SO_2 capacities of selected MOFs are summarized in TABLE 4 and TABLE 5, respectively.

Occurrence and applications

SO_2 is a major air pollutant generated by the combustion of sulfur-containing materials, including coal, sour gas and metal sulfide ores. As SO_2 is a notable contributor to the formation of acid rain and fine particulate matter, it is vital to capture SO_2 from exhaust gases. According to the US Environmental Protection Agency, SO_2 emissions in North America have decreased by 90% over the past 20 years, owing to the implementation of SO_2-removal technologies, such as dry limestone scrubbing and the wet sulfuric acid process[162], yet these processes are not 100% efficient. Thus, coal-fired power plants continue to emit 1.2 million tonnes of SO_2 per year in the USA alone[163]. In addition to the environmental benefits of reducing SO_2 emissions, the complete removal of SO_2 is often crucial prior to contact with downstream catalysts or adsorbent materials intended for other gases to avoid poisoning[164,165]. Consequently, new adsorbent materials that remove SO_2 at low partial pressure are attractive targets in post-combustion exhaust capture, an application that requires extensive cycling stability under humid conditions. Here, we highlight standout examples of MOF stability towards SO_2, as detailed coverage is provided elsewhere[166].

MOFs for SO_2 adsorption

Metal–carboxylate MOFs. Tetravalent metal–carboxylate frameworks can exhibit high uptake capacities for SO_2. For instance, the Zr^{4+} material $[Zr_6(\mu_3\text{-}O)_4(\mu_3\text{-}OH)_4(OH)_4(H_2O)_4(L)_2]$ (MFM-601; L^{4-} = 4,4′,4″,4‴-(1,4-phenylenebis(pyridine-4,2,6-triyl)) tetrabenzoate) adsorbs 12.3 mmol SO_2 g^{-1} MOF at STP[75]. In situ powder X-ray diffraction revealed that this material contains six SO_2 sorption sites, the strongest of which is adjacent to a terminal OH group at the node; however, the adsorption properties of MFM-601 under humid conditions have not been reported. The Ti^{4+} framework Ti-MIL-125 has a high SO_2 uptake capacity of 10.9 mmol g^{-1} under anhydrous conditions at 2.6 bar but decomposes upon exposure to humid SO_2 (REF.[167]). The addition of an NH_2 group to the linker stabilizes the framework under humid conditions and Ti-MIL-125-NH_2 has a comparable SO_2 adsorption capacity of 10.3 mmol g^{-1} at 2.6 bar. Decomposition of Ti-MIL-125 under humid conditions was proposed to result from hydrolysis of the metal–ligand bonds, followed by reaction with SO_2 to form bisulfite (HSO_3^-) and a dangling linker. Density functional theory calculations reveal that the activation energy barrier for hydrolysis of the Ti–O bond in Ti-MIL-125-NH_2 is augmented by ~5 kcal mol^{-1} relative to that in Ti-MIL-125; the additional stabilization is sufficient to slow the decomposition pathway[167].

Trivalent Al^{3+} and In^{3+} carboxylate frameworks reversibly bind dry SO_2 in static adsorption experiments[168–170]. The Al^{3+} carboxylate MOFs, MFM-305-CH_3, MFM-305 and MFM-300 (née NOTT-300), all reversibly adsorb SO_2 with high capacities of >5 mmol g^{-1} (REFS[169,170]). In situ powder X-ray diffraction analysis of MFM-300 revealed that SO_2 strongly interacts with the bridging OH groups of the SBU[169]. A MOF with the more labile In^{3+}, $In(O_2CR)_4$ (NOTT-202a; ^-O_2CR = biphenyl-3,3′,5,5′-tetra-(phenyl-4-carboxylate)), reversibly binds SO_2 with an adsorption capacity of 10 mmol g^{-1} at 1 bar and temperatures between 293 K and 303 K (REF.[168]). However, low-temperature (268–283 K) SO_2 adsorption isotherms feature hysteretic adsorption of an additional 2–6 mmol g^{-1} as a consequence of an irreversible phase change to a denser crystalline polymorph (NOTT-202b). Despite the phase change, SO_2 is completely removed from NOTT-202b at zero pressure, suggesting that SO_2 does not react directly with the framework. The phase change in NOTT-202a has been attributed to the ordering of SO_2 within the pores at adsorption capacities >7 mmol g^{-1}. This process is similar to a pore condensation phenomenon, and the internal pressure created provides enough energy to overcome the activation barrier to transform to the denser NOTT-202b phase, which is 20 kJ mol^{-1} lower in energy than NOTT-202a, owing to increased ligand π stacking within the framework.

Late transition metal–carboxylate frameworks exhibit poor stability towards SO_2. In dynamic breakthrough measurements of Zn^{2+}-based frameworks, MOF-5, MOF-5-NH_2, Zn-MOF-74, MOF-177 and MOF-199, the materials all showed uptake capacities of <0.5 mmol g^{-1}, with the exception of Zn-MOF-74, which adsorbs 3.0 mmol g^{-1}, probably owing to its open metal sites[137]. Increased stability towards dry SO_2 in pillared Zn^{2+} carboxylate MOFs can be achieved by increasing the steric bulk on the linker or by replacing Zn^{2+} with the more inert Ni^{2+} (REFS[70,171]).

The pyridinic coordination networks SIFSIX-1-Cu and SIFSIX-2-Cu-i exhibit high uptakes of dry SO_2 of 11.01 mmol g^{-1} and 6.90 mmol g^{-1}, respectively. The difference in the uptake between the materials is due to the interpenetration of the SIFSIX-2-Cu-i framework. Replacing Cu^{2+} with Zn^{2+} or Ni^{2+} lowers the uptake capacity to 2.10 mmol g^{-1} and 2.74 mmol g^{-1}, respectively. SIFSIX-1-Cu and SIFSIX-2-Cu-i were stable to dry breakthrough testing over 4–6 cycles with mild reactivation parameters of 313 K and a flow of He; however, the stability above 1,000 ppm (~4% RH) of H_2O was not evaluated[172]. The pyridinic frameworks Ni(pyrazine)$_2NbOF_5$ (KAUST-7) and Ni(pyrazine)$_2AlF_5$ (KAUST-8) both exhibit dry uptake capacities of 2.2 mmol g^{-1} when exposed to 7% SO_2 in N_2 and are stable towards SO_2 under humid environments[173].

Metal–azolate MOFs. To date, few metal–azolate frameworks have been explored for SO_2 sorption. One exception is a series of nickel pyrazolate MOFs based on $Ni_8(OH)_4(H_2O)_2(BDP)_6$ (BDP^{2-} = 1,4-benzenedipyrazolate), which show good stability towards SO_2

Table 4 | **Static SO_2 capacities for selected MOFs**

MOF	SO_2 capacity (mmol g^{-1})	Refs
MFM-601	12.3	75
MFM-600	5.0	75
MFM-202[a]	10	168
Ni(BDC)(TED)$_{0.5}$	9.97	171
Zn(BDC)(TED)$_{0.5}$	4.41	171
MOF-74(Mg)	8.60	171
MFM-300(Al) (NOTT-300)	8.1[a]	169
MFM-300(In)	8.3	219
Zn-DMOF-TM	~4.5 (dry)	70
Zn-DMOF-DM	Degrades	70
Zn-DMOF-NDC	~4 (dry)	70
Zn-DMOF-ADC	~5.5 (dry)	70
Cu-DMOF-TM	~2.8 (dry)	70
Ni-DMOF-TM	~5 (dry)	70
Co-DMOF-TM	~3.8 (dry)	70
FMOF-2	1.8	220
MFM-305-CH_3	5.16	170
MFM-305	6.99	170
SIFSIX-1-Cu	11.01	172
SIFSIX-2-Cu-i	6.9	172
Ti-MIL-125	~9.5	167
Ti-MIL-125-NH_2	~9.5	167

Materials tested at 1 bar and 298 K. ADC^{2-}, 9,10-anthracenedicarboxylate; BDC^{2-}, 1,4-benzenedicarboxylate; DM^{2-}, 2,5-dimethyl terephthalate; MOF, metal–organic framework; NDC^{2-}, 1,4-naphthalenedicarboxylate; TED, triethylenediamine; TM^{2-}, tetramethylterephthalate. [a]Measured at 273 K.

Table 5 | **Breakthrough SO_2 capacities for selected MOFs**

MOF	SO_2 concentration (ppm)	SO_2 capacity[a] ($mmol\,g^{-1}$)	Refs
MOF-5	Pure	<0.02	174
IRMOF-3	Pure	0.94	174
Zn-MOF-74	Pure	3.03	174
MOF-177	Pure	<0.02	174
MOF-199	Pure	0.50	174
IRMOF-62	Pure	<0.02	174
SIFSIX-1-Cu	Pure	11.01	172
SIFSIX-2-Cu-i	Pure	6.90	172
SIFSIX-3-Zn	Pure	2.10	172
SIFSIX-3-Ni	Pure	2.74	172
SIFSIX-2-Cu	Pure	6.50	172
Co-MOF-74	382	0.63 (dry)	135
		0.03 (humid)	
Mg-MOF-74	382	1.60 (dry)	135
		0.72 (humid)	
Ni-MOF-74	382	0.04 (dry)	135
		0.02 (humid)	
Zn-MOF-74	382	0.26 (dry)	135
		0.04 (humid)	
$Ni_8(OH)_4(H_2O)_2(BDP\_H)_6$	25,000	2.02	174
$Ni_8(OH)_4(H_2O)_2(BDP\_OH)_6$	25,000	2.11	174
$Ni_8(OH)_4(H_2O)_2(BPD\_NH_2)_6$	25,000	3.35	174
$K[Ni_8(OH)_3(EtO)_3(BDP\_H)_{5.5}]$	25,000	3.26	174
$K_3[Ni_8(OH)_3(EtO)(BDP\_O)_5]$	25,000	2.54	174
$K[Ni_8(OH)_3(EtO)_3(BDP\_NH_2)_{5.5}]$	25,000	4.38	174
$Ba_{0.5}[Ni_8(OH)_3(EtO)_3(BDP\_H)_{5.5}]$	25,000	4.0	174
$Ba_{1.5}[Ni_8(OH)_3(EtO)(BDP\_O)_5]$	25,000	3.65	174
$Ba_{0.5}[Ni_8(OH)_3(EtO)_3(BDP\_NH_2)_{5.5}]$	25,000	5.61	174
$Ni_2\{Ni_4[Cu_2(Me_3mpba)_2]_3\}$	25,000	2.0	221
$Ba_2(H_2O)_9\{Ni_4[Cu_2(Me_3mpba)_2]_3\}$	25,000	2.5	221
$Ni(pyrazine)_2NbOF_5$	70,000	2.2	173
$Ni(pyrazine)_2AlF_5$	70,000	2.2	173

BDP_X^{2-}, 1,4-benzene-dipyrazolate-2-X (X = H, OH or NH_2); Me_3mpba^{2-}, *N*,*N*′-2,4,6-trimethyl-1,3-phenylenebis(oxamate); MOF, metal–organic framework. [a]Measured under dry conditions unless specified otherwise.

(REF.[174]). In dynamic adsorption experiments, the unfunctionalized framework has an SO_2 adsorption capacity of $2.0\,mmol\,g^{-1}$ under 2.5% SO_2 in N_2. The addition of NH_2 or OH groups to the BDP ligand, as well as treatment with a Brønsted base to augment the defect concentration, both increase the SO_2 capacity (TABLE 4). SO_2 binding is not completely reversible within this family of MOFs: the capacity decreases by 26–37% after the first cycle, which has been attributed to the irreversible formation of bisulfite (HSO_3^-) or sulfite (SO_3^{2-}) at the nodes. However, the decay stops after the first cycle and the remaining SO_2 capacity in the second cycle is reversible.

Although no sorption measurements were reported, the stability of several ZIFs under dry and humid SO_2 conditions has been explored[175]. A negligible ~4% decrease in the surface area of ZIF-8 was observed after exposure to dry SO_2; however, the surface area decreases by ~70% after exposure to 20 ppm SO_2 at 85% RH over 10 days. A similar loss of porosity has been observed for other ZIFs, except for ZIF-71 ($Zn(4,5\text{-dichloroimidazolate})_2$), which retains its full pore volume, although it transitions to a dense polymorph in liquid H_2O. Within the ZIFs that lose porosity, analysis by X-ray photoelectron spectroscopy and infrared spectroscopy revealed the formation of HSO_3^- and HSO_4^-, probably due to metal–ligand bond hydrolysis[175].

NO_x

Occurrence and applications

The major components of NO_x are nitrogen monoxide (NO) and nitrogen dioxide (NO_2). These highly toxic species are damaging to respiratory health and contribute to environmental pollution in the troposphere (photochemical smog) and stratosphere (ozone depletion). Anthropogenic NO_x sources are approximately split between agricultural emissions and combustion processes in power plants and automobiles[176]. NO_x emissions are highly regulated and, recently, more stringent regulations are further incentivizing the capture or mitigation of NO_x prior to release[177,178]. Current exhaust systems use catalytic converters to reduce NO_x into N_2 and H_2O, and some MOFs have been investigated for this application[179–182]. However, to achieve further decreases in NO_x emissions, such as during the cold starting of an engine, the exhaust systems of combustion engines require added technologies to adsorb NO or convert NO_x into environmentally benign species. The composition of NO_x from an exhaust engine varies depending on the fuel source; however, the majority of NO_x is initially composed of NO (REF.[183]).

Counterintuitively, given its toxicity, NO has a signalling role in many crucial physiological processes, such as vasodilation, immune defence and neuronal signal transduction[184]. The therapeutic properties of NO have motivated efforts to design materials that release NO under specific, biologically relevant conditions[185,186].

MOFs for NO adsorption

The adsorption of NO has been predominantly tested on MOFs with open metal sites. Studies have mostly focused on MOF materials that store and slowly release low concentrations of NO to improve the performance of medical devices that are in contact with tissues and physiological fluids[185]. For instance, HKUST-1 adsorbs 9 mmol NO g^{-1} MOF at 1 bar and 196 K (REF.[187]). NO interacts directly with the metal, as evidenced by the infrared ν(NO) band at 1,887 cm^{-1}, which is comparable to the infrared bands of Cu^{2+}–NO in molecular complexes[188] and zeolites[189]. The exposure of NO-loaded HKUST-1 to a flow of humid air results in the release of a small amount of NO ($2\,\mu mol\,g^{-1}$) but also leads to a loss in crystallinity. The incorporation of NH_2-functionalized trimesate linkers into HKUST-1 increased the quantity of NO released, but the stability of the MOF remained poor[190].

Biocompatible $Fe_3O(OH)(BDC)_3$ (Fe-MIL-88) and a series of functionalized derivatives adsorb 1–2.5 mmol g^{-1}

with no loss of crystallinity[191]. However, only 5–14% of NO was released upon exposure to humid conditions; most of the NO was likely released prior to the measurement run, suggesting that these materials do not bind NO tightly enough to be stable for long-term storage, which, along with the low NO release dosage, makes them unsuitable for therapeutic applications[191].

The high density of open metal sites in the MOF-74 series makes them attractive for NO sorption studies. The Co^{2+} and Ni^{2+} derivatives each adsorb ~7 mmol g^{-1} and can be stored with NO bound for several months under inert conditions, which is desirable for medical therapies. Flowing humid air through the MOFs results in complete desorption of NO and recovery of the starting material, but these materials are unsuitable for medical applications, as Co^{2+} and Ni^{2+} are not biocompatible[192,193]. Although the Mg^{2+} and Zn^{2+} MOF-74 analogues are biocompatible, Mg-MOF-74 binds NO too strongly, with NO only being released at <11% RH, whereas Zn-MOF-74 loses NO too readily under preparatory conditions. The quantity and rate of deliverable NO can, however, be tuned by doping Mg-MOF-74 with up to 40% Ni^{2+} (REF.[194]). Fe-MOF-74 adsorbs 6.21 mmol g^{-1} at 7 mbar, which corresponds to 95% occupation of the Fe^{2+} open metals sites by NO (REF.[195]). Under a flow of 11% RH in N_2, the bound NO is released gradually over a period of days[195].

MOFs for NO_2 adsorption

There are limited reports of NO_2 adsorption in MOFs. The Zr^{4+} carboxylate frameworks UiO-66 and UiO-67 capture 7.3 wt% and 7.9 wt% NO_2, respectively, under 1,000 ppm dry NO_2, and the capacity of UiO-67 is augmented to 11.8 wt% under 71% RH, possibly owing to NO_2 dissolution into pore-confined H_2O. Furthermore, functionalization of the linker of UiO-66 with NH_2 increases the static NO_2 capacity fivefold[196,197]. Characterization of UiO-66-NH_2 following NO_2 adsorption using infrared and ^{1}H NMR spectroscopy indicates that the mechanism of NO_2 removal occurs through a complicated set of reaction pathways that involve the reaction of NH_2 groups to form diazonium ions and the nitrosation of phenyl C–H bonds[197]. Indeed, NO_2 adsorption is not reversible in UiO-66-type frameworks and it has been proposed that NO_2 reacts at the Zr–O–Zr bridges, resulting in partial framework collapse[196].

Reversible NO_2 capture was achieved in the Al^{3+} carboxylate MOF, MFM-300, which adsorbs 14.1 mmol NO_2 g^{-1} MOF over five cycles, with no loss in capacity or crystallinity. Analysis of a NO_2-loaded sample using synchrotron powder X-ray diffraction revealed a 1D helical chain of NO_2 and N_2O_4 units within the pores. Each NO_2 forms five weak interactions with the framework, a consequence of the precisely tailored pore size, which stabilize the helical chain. Additionally, MFM-300 exhibits preferential binding of NO_2 over CO_2 and SO_2. Notably, under wet conditions (with 0.5% NO_2 in N_2), the NO_2 breakthrough time decreases by ~10% compared with that in dry conditions; this decline is postulated to result from competitive binding between H_2O and NO_2. Analysis of the material post-breakthrough experiment was not detailed[198].

The addition of NO_2 to a Zr^{4+} carboxylate MOF featuring a calixarene linker results in partial formation of N_2O_4 and subsequent disproportionation to NO^+ and NO_3^-. The resulting NO^+ transfers to the calixarene linker, generating a strongly adsorbed donor–acceptor complex that is detectable using calorimetry. The process appears to be reversible and the material retained crystallinity after repeated NO_2 exposure[199].

Halogens

Occurrence and applications

Motivated by the capture of volatile radioisotopes of I_2 from nuclear waste streams, most research on the adsorption of halogens by MOFs has focused on I_2 (REFS[200–207]). Here, we focus on the more volatile halogens Cl_2 and Br_2, which are less commonly explored, although the capture and reversible storage of these highly toxic gases is central to improving PPE and increasing the safety of handling, storing and transporting these gases.

MOFs for halogen adsorption

Unfunctionalized carboxylate frameworks, including MOF-5, UiO-66 and Al-MIL-53, exhibit negligible Cl_2 uptake under dynamic conditions (3 wt% and 1 wt% for UiO-66 and Al-MIL-53, respectively)[137]. Functionalization of the terephthalate ligand improves Cl_2 uptake but only when the aromatic ring is sufficiently activated towards electrophilic aromatic substitution. For instance, functionalization of UiO-66 with OH groups results in a negligible improvement in Cl_2 uptake to 5 wt%. By contrast, the addition of an NH_2 group to the terephthalate linker enhances Cl_2 uptake by an order of magnitude in MOF-5-NH_2 (35.5 wt%)[137], UiO-66-NH_2 (154 wt%) and Al-MIL-53-NH_2 (56 wt%)[208]. The NH_2 groups have a dual function: they strongly activate the terephthalate linker to electrophilic aromatic substitution, leading to chlorination of the ring and formation of HCl, and also neutralize HCl to form $–NH_3Cl$; this is an irreversible process that cannot be used cyclically.

Reversible storage of the lighter halogens was demonstrated using Co_2Cl_2BTDD[209]. The cobalt metal centres are redox-active with an accessible Co(II/III) redox couple that is suitable for reactions with Cl_2 and Br_2. Exposure of Co_2Cl_2BTDD to Cl_2 or Br_2 results in the oxidation of five-coordinate Co^{2+} to octahedral Co^{3+}, forming $Co_2Cl_2X_2$BTDD (X = Cl or Br), while maintaining crystallinity and porosity (FIG. 6). Heating $Co_2Cl_2X_2$BTDD to 275 °C (X = Cl) or 195 °C (X = Br) results in the reductive release of the X_2 gas and reformation of the parent Co_2Cl_2BTDD (FIG. 6). The capture and release of Br_2 was repeated over three cycles with reproducible yields of 75–80% on the initial cycle and 100% yield on subsequent ones[209]. The exceptional stability of Co_2Cl_2BTDD towards X_2 is attributed to strong metal–ligand bonds, open metal sites with an accessible Co(II/III) redox couple and particularly strong aromatic C–H bonds that are not susceptible to radical attack. After oxidation, the framework stability may increase, as the rate of ligand exchange for Co^{3+} is eight orders of magnitude slower than that of Co^{2+}.

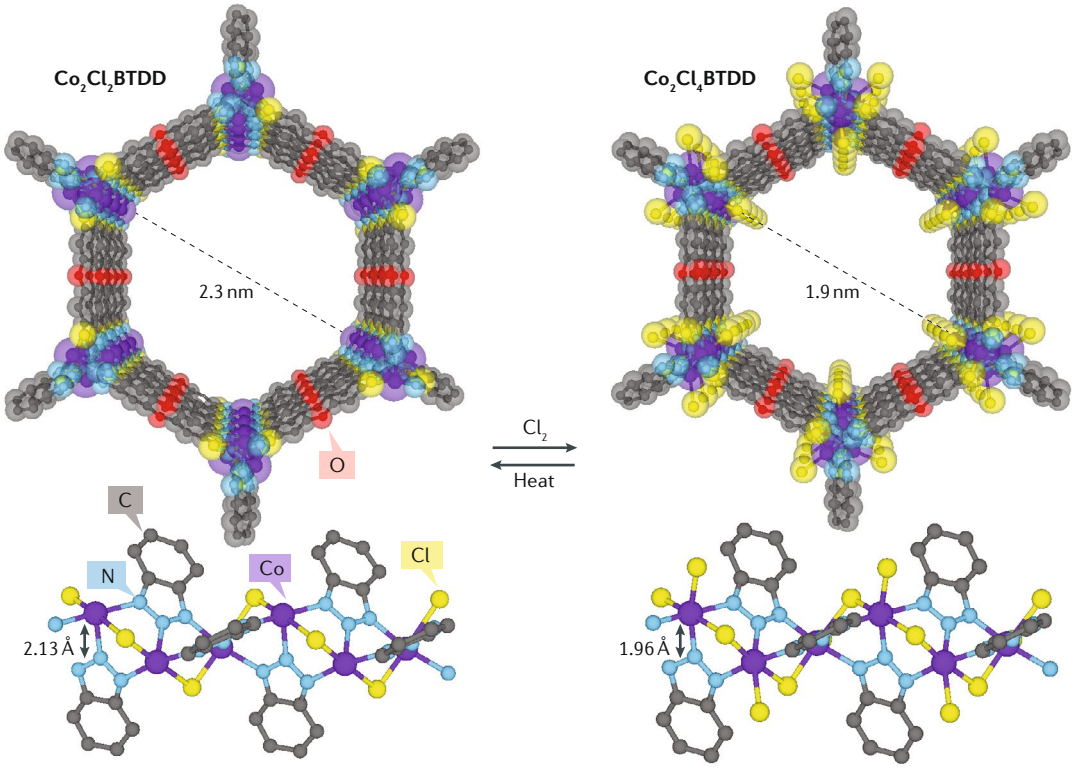

Fig. 6 | **Oxidative capture of halogens.** Co_2Cl_2BTDD ($BTDD^{2-}$ = bis(1*H*-1,2,3-triazolato[4,5-b],[4′,5′-i])dibenzo[1,4]dioxin) captures Cl_2 (or Br_2) through reversible oxidation to Co_2Cl_4BTDD (or $Co_2Cl_2Br_2BTDD$). H atoms omitted for clarity.

Outlook

It is frequently cost-prohibitive to remove all H_2O, NH_3, H_2S or SO_x and/or NO_x from the atmosphere or from feed gas streams, necessitating that MOFs used in applications such as CO_2 removal from flue gas have long-term stability to coordinating and corrosive species. Additionally, although we have divided this Review into separate sections on each analyte gas, these species are often present together, which may give rise to other challenges, such as the formation of H_2SO_4 from SO_x, H_2O and O_2. Multicomponent stability testing has largely been overlooked thus far, but it is vital for real-world applications. The design of frameworks for the capture of these challenging gases pushes the boundaries of sorbent robustness and advances our understanding of the fundamental kinetics and thermodynamics of MOF stability.

MOFs are typically synthesized from weakly donating ligands, such as carboxylates, in combination with labile metal ions, such as Zn^{2+} and Cu^{2+}. Together, these components favour reversible ligand binding to promote ideal crystal growth. The crystallization of MOFs using inert metal ions, such as Cr^{3+}, or more strongly donating ligands, such as pyrazolates, is more difficult because the reversible sampling of configurations towards the local minimum-energy state is not as efficient. Therefore, harsh synthetic conditions such as high temperature, high pressure and the use of mineralizers such as HF are often required[30]. Consequently, it becomes more difficult to obtain large crystals, complicating structure determination. Indeed, the structures in the original reports of Cr-MIL-53 and Cr-MIL-101 were solved using powder refinement rather than by more straightforward single-crystal methods, which require larger cystals[30,31]. Although the synthesis of MOFs containing inert metals, or ligands that are more strongly donating, can be challenging[210,211], it may lead to structures capable of withstanding demanding conditions relevant for many applications. Ultimately, nothing good comes easy: in general, MOFs that crystallize easily and therefore grow as large, single crystals are less stable to H_2O or other corrosive and coordinating gases.

Porous materials are kinetically stable. Currently, the default vocabulary for describing the stability of MOFs is a binary scale: stable versus unstable. Moving forward, our view is that MOFs should be ranked on a continuum of kinetic stability. Quantitative benchmarking of all MOFs using a broadly applicable stability rating, such as those already used for a limited number of MOFs based on H_2O vapour or steam temperature[50,212], could advance the field by enabling facile material selection based on application-specific stability requirements. Recent research has followed two main paths to stabilize the porous phase: engineering heterolytically stronger metal–ligand bonds or using more inert metals. These approaches have led to exceptionally robust frameworks, which portend the use of MOFs for applications requiring extensive stability towards harsh gases and vapours, as well as in areas requiring long-term lower-level stability. Future progress in this direction will enable MOFs to fulfil their promise as designer multifunctional materials for diverse applications.

Published online: 13 September 2019

1. Furukawa, H., Cordova, K. E., O'Keeffe, M. & Yaghi, O. M. The chemistry and applications of metal-organic frameworks. *Science* **341**, 1230444 (2013).
2. Mason, J. A., Veenstra, M. & Long, J. R. Evaluating metal–organic frameworks for natural gas storage. *Chem. Sci.* **5**, 32–51 (2014).
3. Murray, L. J., Dincă, M. & Long, J. R. Hydrogen storage in metal–organic frameworks. *Chem. Soc. Rev.* **38**, 1294–1314 (2009).
4. DeSantis, D. et al. Techno-economic analysis of metal–organic frameworks for hydrogen and natural gas storage. *Energy Fuels* **31**, 2024–2032 (2017).
5. Yoon, J. W. et al. Selective nitrogen capture by porous hybrid materials containing accessible transition metal ion sites. *Nat. Mater.* **16**, 526–531 (2017).
6. Kizzie, A. C., Wong-Foy, A. G. & Matzger, A. J. Effect of humidity on the performance of microporous coordination polymers as adsorbents for CO_2 capture. *Langmuir* **27**, 6368–6373 (2011).
7. Adil, K. et al. Gas/vapour separation using ultra-microporous metal–organic frameworks: insights into the structure/separation relationship. *Chem. Soc. Rev.* **46**, 3402–3430 (2017).
8. Dusselier, M. & Davis, M. E. Small-pore zeolites: synthesis and catalysis. *Chem. Rev.* **118**, 5265–5329 (2018).
9. Yang, D. & Gates, B. C. Catalysis by metal organic frameworks: perspective and suggestions for future research. *ACS Catal.* **9**, 1779–1798 (2019).
10. Lee, J. et al. Metal–organic framework materials as catalysts. *Chem. Soc. Rev.* **38**, 1450–1459 (2009).
11. Sun, L., Campbell, M. G. & Dincă, M. Electrically conductive porous metal–organic frameworks. *Angew. Chem. Int. Ed.* **55**, 3566–3579 (2016).
12. Hendon, C. H., Rieth, A. J., Korzyński, M. D. & Dincă, M. Grand challenges and future opportunities for metal–organic frameworks. *ACS Cent. Sci.* **3**, 554–563 (2017).
13. Furukawa, H. et al. Ultrahigh porosity in metal–organic frameworks. *Science* **329**, 424–428 (2010).
14. Kitagawa, S. Porous materials and the age of gas. *Angew. Chem. Int. Ed.* **54**, 10686–10687 (2015).
15. Cheetham, A. K., Kieslich, G. & Yeung, H. H. M. Thermodynamic and kinetic effects in the crystallization of metal–organic frameworks. *Acc. Chem. Res.* **51**, 659–667 (2018).
16. Hughes, J. T. & Navrotsky, A. MOF-5: enthalpy of formation and energy landscape of porous materials. *J. Am. Chem. Soc.* **133**, 9184–9187 (2011).
17. Hughes, J. T., Bennett, T. D., Cheetham, A. K. & Navrotsky, A. Thermochemistry of zeolitic imidazolate frameworks of varying porosity. *J. Am. Chem. Soc.* **135**, 598–601 (2013).
Study in which calorimetric measurements indicate that evacuated porous phases of many ZIFs, along with previously measured MOF-5, zeolites and mesoporous silicas, are metastable with respect to dense phases of the same components.
18. Bhunia, M. K., Hughes, J. T., Fettinger, J. C. & Navrotsky, A. Thermochemistry of paddle wheel MOFs: Cu-HKUST-1 and Zn-HKUST-1. *Langmuir* **29**, 8140–8145 (2013).
19. Wu, L., Hughes, J., Moliner, M., Navrotsky, A. & Corma, A. Experimental energetics of large and extra-large pore zeolites: pure silica beta polymorph C (BEC) and Ge-containing ITQ-33. *Microporous Mesoporous Mater.* **187**, 77–81 (2014).
20. Akimbekov, Z. & Navrotsky, A. Little thermodynamic penalty for the synthesis of ultraporous metal organic frameworks. *ChemPhysChem* **17**, 468–470 (2016).
21. Akimbekov, Z., Wu, D., Brozek, C. K., Dincă, M. & Navrotsky, A. Thermodynamics of solvent interaction with the metal–organic framework MOF-5. *Phys. Chem. Chem. Phys.* **18**, 1158–1162 (2015).
22. Bennett, T. D. & Horike, S. Liquid, glass and amorphous solid states of coordination polymers and metal–organic frameworks. *Nat. Rev. Mater.* **3**, 431–440 (2018).
23. Zhou, C. et al. Thermodynamic features and enthalpy relaxation in a metal–organic framework glass. *Phys. Chem. Chem. Phys.* **20**, 18291–18296 (2018).
24. Keen, D. A. & Bennett, T. D. Structural investigations of amorphous metal–organic frameworks formed via different routes. *Phys. Chem. Chem. Phys.* **20**, 7857–7861 (2018).
25. Longley, L. et al. Flux melting of metal–organic frameworks. *Chem. Sci.* **10**, 3592–3601 (2019).
26. Hu, Y. H. & Zhang, L. Amorphization of metal-organic framework MOF-5 at unusually low applied pressure. *Phys. Rev. B* **81**, 174103 (2010).
27. Erkartal, M. & Durandurdu, M. Pressure-induced amorphization of MOF-5: a first principles study. *ChemistrySelect* **3**, 8056–8063 (2018).
28. Bennett, T. D. et al. Reversible pressure-induced amorphization of a zeolitic imidazolate framework (ZIF-4). *Chem. Commun.* **47**, 7983–7985 (2011).
29. Eigen, M. Fast elementary steps in chemical reaction mechanisms. *Pure Appl. Chem.* **6**, 97–115 (1963).
30. Férey, G. et al. A chromium terephthalate-based solid with unusually large pore volumes and surface area. *Science* **309**, 2040–2042 (2005).
31. Millange, F., Serre, C. & Férey, G. Synthesis, structure determination and properties of MIL-53as and MIL-53ht: The first Cr^{III} hybrid inorganic–organic microporous solids: $Cr^{III}(OH)\cdot\{O_2C–C_6H_4–CO_2\}\cdot\{HO_2C–C_6H_4–CO_2H\}_x$. *Chem. Commun.* **8**, 822–823 (2002).
32. Hamon, L. et al. Molecular insight into the adsorption of H_2S in the flexible MIL-53(Cr) and rigid MIL-47(V) MOFs: infrared spectroscopy combined to molecular simulations. *J. Phys. Chem. C* **115**, 2047–2056 (2011).
33. Kang, I. J., Khan, N. A., Haque, E. & Jhung, S. H. Chemical and thermal stability of isotypic metal–organic frameworks: effect of metal ions. *Chem. Eur. J.* **17**, 6437–6442 (2011).
Study showing that the trend in chemical stability for a family of isostructural carboxylate frameworks is in line with the kinetics of metal–ligand exchange but contrasts with the trend in metal–oxygen bond strength.
34. Rosi, N. L. et al. Rod packings and metal–organic frameworks constructed from rod-shaped secondary building units. *J. Am. Chem. Soc.* **127**, 1504–1518 (2005).
35. Dietzel, P. D. C., Panella, B., Hirscher, M., Blom, R. & Fjellvåg, H. Hydrogen adsorption in a nickel based coordination polymer with open metal sites in the cylindrical cavities of the desolvated framework. *Chem. Commun.* **9**, 959–961 (2006).
36. Jiao, Y. et al. Tuning the kinetic water stability and adsorption interactions of Mg-MOF-74 by partial substitution with Co or Ni. *Ind. Eng. Chem. Res.* **54**, 12408–12414 (2015).
37. Li, H. et al. Enhanced hydrostability in Ni-doped MOF-5. *Inorg. Chem.* **51**, 9200–9207 (2012).
38. Liao, P.-Q. et al. Drastic enhancement of catalytic activity via post-oxidation of a porous Mn^{II} triazolate framework. *Chem. Eur. J.* **20**, 11303–11307 (2014).
39. Liao, P.-Q. et al. Monodentate hydroxide as a super strong yet reversible active site for CO_2 capture from high-humidity flue gas. *Energy Environ. Sci.* **8**, 1011–1016 (2015).
40. Rieth, A. J., Tulchinsky, Y. & Dincă, M. High and reversible ammonia uptake in mesoporous azolate metal–organic frameworks with open Mn, Co, and Ni sites. *J. Am. Chem. Soc.* **138**, 9401–9404 (2016).
41. Rieth, A. J., Yang, S., Wang, E. N. & Dincă, M. Record atmospheric fresh water capture and heat transfer with a material operating at the water uptake reversibility limit. *ACS Cent. Sci.* **3**, 668–672 (2017).
Study in which a family of triazolate MOFs with pore diameters greater than the size at which irreversibility upon H_2O desorption is expected nevertheless exhibits reversible H_2O isotherms, owing to adsorption of H_2O at open metal sites prior to the pore-filling event.
42. Rieth, A. J. & Dincă, M. Controlled gas uptake in metal–organic frameworks with record ammonia sorption. *J. Am. Chem. Soc.* **140**, 3461–3466 (2018).
Study showing that triazolate MOFs that exhibit a high density of open metal sites sorb record amounts of NH_3 and that the trend in stability towards NH_3 for the Mn^{2+}, Co^{2+}, Ni^{2+} and Cu^{2+} materials follows the trend in metal cation inertness.
43. Rieth, A. J. et al. Tunable metal–organic frameworks enable high-efficiency cascaded adsorption heat pumps. *J. Am. Chem. Soc.* **140**, 17591–17596 (2018).
44. Irving, H. & Williams, R. J. P. Order of stability of metal complexes. *Nature* **162**, 746–747 (1948).
45. Irving, H. & Williams, R. J. P. The stability of transition-metal complexes. *J. Chem. Soc.* 3192–3210 (1953).
46. Choi, H. J., Dincă, M. & Long, J. R. Broadly hysteretic H_2 adsorption in the microporous metal–organic framework Co(1,4-benzenedipyrazolate). *J. Am. Chem. Soc.* **130**, 7848–7850 (2008).
47. Choi, H. J., Dincă, M., Dailly, A. & Long, J. R. Hydrogen storage in water-stable metal–organic frameworks incorporating 1,3- and 1,4-benzenedipyrazolate. *Energy Environ. Sci.* **3**, 117–123 (2010).
48. Wade, C. R., Corrales-Sanchez, T., Narayan, T. C. & Dincă, M. Postsynthetic tuning of hydrophilicity in pyrazolate MOFs to modulate water adsorption properties. *Energy Environ. Sci.* **6**, 2172–2177 (2013).
49. Colombo, V. et al. High thermal and chemical stability in pyrazolate-bridged metal–organic frameworks with exposed metal sites. *Chem. Sci.* **2**, 1311–1319 (2011).
50. Low, J. J. et al. Virtual high throughput screening confirmed experimentally: porous coordination polymer hydration. *J. Am. Chem. Soc.* **131**, 15834–15842 (2009).
Study in which the experimental evidence and theoretical calculations reveal that hydrolysis of metal–ligand bonds is favourable and has a similar driving force for diverse frameworks, including MOF-5, ZIF-8 and HKUST-1, but that the activation energy barrier for hydrolysis is the determining factor for hydrothermal stability.
51. Olmstead, W. N., Margolin, Z. & Bordwell, F. G. Acidities of water and simple alcohols in dimethyl sulfoxide solution. *J. Org. Chem.* **45**, 3295–3299 (1980).
52. Bordwell, F. G. Equilibrium acidities in dimethyl sulfoxide solution. *Acc. Chem. Res.* **21**, 456–463 (1988).
53. Mondloch, J. E. et al. Vapor-phase metalation by atomic layer deposition in a metal–organic framework. *J. Am. Chem. Soc.* **135**, 10294–10297 (2013).
54. Cavka, J. H. et al. A new zirconium inorganic building brick forming metal organic frameworks with exceptional stability. *J. Am. Chem. Soc.* **130**, 13850–13851 (2008).
55. Furukawa, H. et al. Water adsorption in porous metal–organic frameworks and related materials. *J. Am. Chem. Soc.* **136**, 4369–4381 (2014).
56. Li, H., Cosio, M., Wang, K., Burtner, W. & Zhou, H.-C. in *Elaboration and Applications of Metal-Organic Frameworks* Ch. 1 (eds Ma, S. & Perman, J. A.) 1–35 (World Scientific, 2018).
57. Burtch, N. C., Jasuja, H. & Walton, K. S. Water stability and adsorption in metal–organic frameworks. *Chem. Rev.* **114**, 10575–10612 (2014).
58. Nguyen, J. G. & Cohen, S. M. Moisture-resistant and superhydrophobic metal–organic frameworks obtained via postsynthetic modification. *J. Am. Chem. Soc.* **132**, 4560–4561 (2010).
59. Li, T. et al. Systematic modulation and enhancement of CO_2:N_2 selectivity and water stability in an isoreticular series of bio-MOF-11 analogues. *Chem. Sci.* **4**, 1746–1755 (2013).
60. Makal, T. A., Wang, X. & Zhou, H.-C. Tuning the moisture and thermal stability of metal–organic frameworks through incorporation of pendant hydrophobic groups. *Cryst. Growth Des.* **13**, 4760–4768 (2013).
61. Jasuja, H., Huang, Y. & Walton, K. S. Adjusting the stability of metal–organic frameworks under humid conditions by ligand functionalization. *Langmuir* **28**, 16874–16880 (2012).
62. Tan, K. et al. Water reaction mechanism in metal organic frameworks with coordinatively unsaturated metal ions: MOF-74. *Chem. Mater.* **26**, 6886–6895 (2014).
63. Al-Janabi, N., Alfutimie, A., Siperstein, F. R. & Fan, X. Underlying mechanism of the hydrothermal instability of $Cu_3(BTC)_2$ metal-organic framework. *Front. Chem. Sci. Eng.* **10**, 103–107 (2016).
64. Gul-E-Noor, F. et al. Effects of varying water adsorption on a $Cu_3(BTC)_2$ metal–organic framework (MOF) as studied by ^1H and ^{13}C solid-state NMR spectroscopy. *Phys. Chem. Chem. Phys.* **13**, 7783–7788 (2011).
65. McHugh, L. N. et al. Hydrolytic stability in hemilabile metal–organic frameworks. *Nat. Chem.* **10**, 1096–1102 (2018).
66. Tian, Y. et al. Synthesis and structural characterization of a single-crystal to single-crystal transformable coordination polymer. *Dalton Trans.* **43**, 1519–1523 (2014).
67. Towsif Abtab, S. M. et al. Reticular chemistry in action: a hydrolytically stable MOF capturing twice its weight in adsorbed water. *Chem* **4**, 94–105 (2018).
Study reporting a mesoporous Cr^{3+} carboxylate framework that has a record 200 wt% capacity

for H_2O and can cyclically capture H_2O, whereas isostructural frameworks formed with more labile cations, such as Fe^{3+} or Al^{3+}, collapse upon H_2O uptake.
68. Howarth, A. J. et al. Chemical, thermal and mechanical stabilities of metal–organic frameworks. *Nat. Rev. Mater.* **1**, 15018 (2016).
69. Peterson, G. W. et al. Ammonia vapor removal by $Cu_3(BTC)_2$ and its characterization by MAS NMR. *J. Phys. Chem. C* **113**, 13906–13917 (2009).
70. Hungerford, J. et al. DMOF-1 as a representative MOF for SO_2 adsorption in both humid and dry conditions. *J. Phys. Chem. C* **122**, 23493–23500 (2018).
71. Ruhl, A. S. & Kranzmann, A. Investigation of corrosive effects of sulphur dioxide, oxygen and water vapour on pipeline steels. *Int. J. Greenh. Gas Con.* **13**, 9–16 (2013).
72. Elder, A. C., Bhattacharyya, S., Nair, S. & Orlando, T. M. Reactive adsorption of humid SO_2 on metal–organic framework nanosheets. *J. Phys. Chem. C* **122**, 10413–10422 (2018).
73. Brozek, C. K., Miller, J. T., Stoian, S. A. & Dincă, M. NO disproportionation at a mononuclear site-isolated Fe^{2+} center in Fe^{2+}-MOF-5. *J. Am. Chem. Soc.* **137**, 7495–7501 (2015).
74. McGrath, D. T. et al. Selective decontamination of the reactive air pollutant nitrous acid via node-linker cooperativity in a metal-organic framework. *Chem. Sci.* **10**, 5576–5581 (2019).
75. Carter, J. H. et al. Exceptional adsorption and binding of sulfur dioxide in a robust zirconium-based metal–organic framework. *J. Am. Chem. Soc.* **140**, 15564–15567 (2018).
76. Canivet, J., Fateeva, A., Guo, Y., Coasne, B. & Farrusseng, D. Water adsorption in MOFs: fundamentals and applications. *Chem. Soc. Rev.* **43**, 5594–5617 (2014).
77. Liu, J. et al. Stability effects on CO_2 adsorption for the DOBDC series of metal–organic frameworks. *Langmuir* **27**, 11451–11456 (2011).
78. Campbell, M. G., Sheberla, D., Liu, S. F., Swager, T. M. & Dincă, M. Cu_3(hexaiminotriphenylene)$_2$: an electrically conductive 2D metal–organic framework for chemiresistive sensing. *Angew. Chem. Int. Ed.* **54**, 4349–4352 (2015).
79. Park, S. S., Rieth, A. J., Hendon, C. H. & Dincă, M. Selective vapor pressure dependent proton transport in a metal–organic framework with two distinct hydrophilic pores. *J. Am. Chem. Soc.* **140**, 2016–2019 (2018).
80. Cui, S. et al. Metal-organic frameworks as advanced moisture sorbents for energy-efficient high temperature cooling. *Sci. Rep.* **8**, 15284 (2018).
81. Abdulhalim, R. G. et al. A fine-tuned metal-organic framework for autonomous indoor moisture control. *J. Am. Chem. Soc.* **139**, 10715–10722 (2017).
82. Critoph, R. E. Evaluation of alternative refrigerant–adsorbent pairs for refrigeration cycles. *Appl. Therm. Eng.* **16**, 891–900 (1996).
83. De Lange, M. F., Verouden, K. J. F. M., Vlugt, T. J. H., Gascon, J. & Kapteijn, F. Adsorption-driven heat pumps: the potential of metal–organic frameworks. *Chem. Rev.* **115**, 12205–12250 (2015).
84. Kalmutzki, M. J., Diercks, C. S. & Yaghi, O. M. Metal–organic frameworks for water harvesting from air. *Adv. Mater.* **30**, 1704304 (2018).
85. Trapani, F., Polyzoidis, A., Loebbecke, S. & Piscopo, C. G. On the general water harvesting capability of metal-organic frameworks under well-defined climatic conditions. *Microporous Mesoporous Mater.* **230**, 20–24 (2016).
86. Kim, H. et al. Adsorption-based atmospheric water harvesting device for arid climates. *Nat. Commun.* **9**, 1191 (2018).
87. Kim, H. et al. Water harvesting from air with metal-organic frameworks powered by natural sunlight. *Science* **356**, 430–434 (2017).
The first report of a device with a MOF (MOF-801) that captures H_2O from the atmosphere and can be regenerated using low-grade heat from natural sunlight.
88. Fathieh, F. et al. Practical water production from desert air. *Sci. Adv.* **4**, eaat3198 (2018).
89. Canivet, J. et al. Structure–property relationships of water adsorption in metal–organic frameworks. *New J. Chem.* **38**, 3102–3111 (2014).
90. Jeremias, F., Lozan, V., Henninger, S. K. & Janiak, C. Programming MOFs for water sorption: amino-functionalized MIL-125 and UiO-66 for heat transformation and heat storage applications. *Dalton Trans.* **42**, 15967–15973 (2013).
91. Akiyama, G. et al. Effect of functional groups in MIL-101 on water sorption behavior. *Microporous Mesoporous Mater.* **157**, 89–93 (2012).
92. Khutia, A., Rammelberg, H. U., Schmidt, T., Henninger, S. & Janiak, C. Water sorption cycle measurements on functionalized MIL-101Cr for heat transformation application. *Chem. Mater.* **25**, 790–798 (2013).
93. Wright, A. M., Rieth, A. J., Yang, S., Wang, E. & Dincă, M. Precise control of pore hydrophilicity enabled by post-synthetic cation exchange in metal–organic frameworks. *Chem. Sci.* **9**, 3856–3859 (2018).
94. Rieth, A. J. et al. Record-setting sorbents for reversible water uptake by systematic anion exchanges in metal–organic frameworks. *J. Am. Chem. Soc.* **141**, 13858–13866 (2019).
95. Jasuja, H., Zang, J., Sholl, D. S. & Walton, K. S. Rational tuning of water vapor and CO_2 adsorption in highly stable Zr-based MOFs. *J. Phys. Chem. C* **116**, 23526–23532 (2012).
96. Wißmann, G. et al. Modulated synthesis of Zr-fumarate MOF. *Microporous Mesoporous Mater.* **152**, 64–70 (2012).
97. Schaate, A. et al. Porous interpenetrated zirconium–organic frameworks (PIZOFs): a chemically versatile family of metal–organic frameworks. *Chem. Eur. J.* **17**, 9320–9325 (2011).
98. DeCoste, J. B., Demasky, T. J., Katz, M. J., Farha, O. K. & Hupp, J. T. A UiO-66 analogue with uncoordinated carboxylic acids for the broad-spectrum removal of toxic chemicals. *New J. Chem.* **39**, 2396–2399 (2015).
99. Wu, H. et al. Unusual and highly tunable missing-linker defects in zirconium metal–organic framework UiO-66 and their important effects on gas adsorption. *J. Am. Chem. Soc.* **135**, 10525–10532 (2013).
100. Vermoortele, F. et al. Synthesis modulation as a tool to increase the catalytic activity of metal–organic frameworks: the unique case of UiO-66(Zr). *J. Am. Chem. Soc.* **135**, 11465–11468 (2013).
101. Shearer, G. C. et al. Defect engineering: tuning the porosity and composition of the metal–organic framework UiO-66 via modulated synthesis. *Chem. Mater.* **28**, 3749–3761 (2016).
102. Wang, S. et al. A robust large-pore zirconium carboxylate metal–organic framework for energy-efficient water-sorption-driven refrigeration. *Nat. Energy* **3**, 985–993 (2018).
103. Volkringer, C. et al. Synthesis, single-crystal X-ray microdiffraction, and NMR characterizations of the giant pore metal-organic framework aluminum trimesate MIL-100. *Chem. Mater.* **21**, 5695–5697 (2009).
104. Jeremias, F., Khutia, A., Henninger, S. K. & Janiak, C. MIL-100(Al, Fe) as water adsorbents for heat transformation purposes—a promising application. *J. Mater. Chem.* **22**, 10148–10151 (2012).
105. Loiseau, T. et al. A rationale for the large breathing of the porous aluminum terephthalate (MIL-53) upon hydration. *Chem. Eur. J.* **10**, 1373–1382 (2004).
106. Kummer, H. et al. A functional full-scale heat exchanger coated with aluminum fumarate metal–organic framework for adsorption heat transformation. *Ind. Eng. Chem. Res.* **56**, 8393–8398 (2017).
107. Fröhlich, D. et al. Water adsorption behaviour of CAU-10-H: a thorough investigation of its structure–property relationships. *J. Mater. Chem. A* **4**, 11859–11869 (2016).
108. Fröhlich, D., Henninger, S. K. & Janiak, C. Multicycle water vapour stability of microporous breathing MOF aluminium isophthalate CAU-10-H. *Dalton Trans.* **43**, 15300–15304 (2014).
109. Reinsch, H. et al. Structures, sorption characteristics, and nonlinear optical properties of a new series of highly stable aluminum MOFs. *Chem. Mater.* **25**, 17–26 (2013).
110. Lenzen, D. et al. Scalable green synthesis and full-scale test of the metal–organic framework CAU-10-H for use in adsorption-driven chillers. *Adv. Mater.* **30**, 1705869 (2018).
111. Cadiau, A. et al. Design of hydrophilic metal organic framework water adsorbents for heat reallocation. *Adv. Mater.* **27**, 4775–4780 (2015).
112. Küsgens, P. et al. Characterization of metal-organic frameworks by water adsorption. *Microporous Mesoporous Mater.* **120**, 325–330 (2009).
113. Ehrenmann, J., Henninger, S. K. & Janiak, C. Water adsorption characteristics of MIL-101 for heat-transformation applications of MOFs. *Eur. J. Inorg. Chem.* **2011**, 471–474 (2011).
114. Seo, Y.-K. et al. Energy-efficient dehumidification over hierachically porous metal–organic frameworks as advanced water adsorbents. *Adv. Mater.* **24**, 806–810 (2012).
115. Alezi, D. et al. MOF crystal chemistry paving the way to gas storage needs: aluminum-based soc-MOF for CH_4, O_2, and CO_2 storage. *J. Am. Chem. Soc.* **137**, 13308–13318 (2015).
116. Chen, Z. et al. Reticular access to highly porous acs-MOFs with rigid trigonal prismatic linkers for water sorption. *J. Am. Chem. Soc.* **141**, 2900–2905 (2019).
117. Sohail, M. et al. Synthesis of highly crystalline NH_2-MIL-125 (Ti) with S-shaped water isotherms for adsorption heat transformation. *Cryst. Growth Des.* **17**, 1208–1213 (2017).
118. Masciocchi, N. et al. Cubic octanuclear Ni(II) clusters in highly porous polypyrazolyl-based materials. *J. Am. Chem. Soc.* **132**, 7902–7904 (2010).
119. Wang, K. et al. Pyrazolate-based porphyrinic metal–organic framework with extraordinary base-resistance. *J. Am. Chem. Soc.* **138**, 914–919 (2016).
120. Padial, N. M. et al. Highly hydrophobic isoreticular porous metal–organic frameworks for the capture of harmful volatile organic compounds. *Angew. Chem. Int. Ed.* **52**, 8290–8294 (2013).
121. Denysenko, D. et al. Elucidating gating effects for hydrogen sorption in MFU-4-type triazolate-based metal–organic frameworks featuring different pore sizes. *Chem. Eur. J.* **17**, 1837–1848 (2011).
122. Denysenko, D., Grzywa, M., Jelic, J., Reuter, K. & Volkmer, D. Scorpionate-type coordination in MFU-4*l* metal–organic frameworks: small-molecule binding and activation upon the thermally activated formation of open metal sites. *Angew. Chem. Int. Ed.* **53**, 5832–5836 (2014).
123. Shustova, N. B., Cozzolino, A. F., Reineke, S., Baldo, M. & Dincă, M. Selective turn-on ammonia sensing enabled by high-temperature fluorescence in metal–organic frameworks with open metal sites. *J. Am. Chem. Soc.* **135**, 13326–13329 (2013).
124. Smith, M. K., Jensen, K. E., Pivak, P. A. & Mirica, K. A. Direct self-assembly of conductive nanorods of metal–organic frameworks into chemiresistive devices on shrinkable polymer films. *Chem. Mater.* **28**, 5264–5268 (2016).
125. Bobbitt, N. S. et al. Metal–organic frameworks for the removal of toxic industrial chemicals and chemical warfare agents. *Chem. Soc. Rev.* **46**, 3357–3385 (2017).
126. Chen, Y., Li, L., Li, J., Ouyang, K. & Yang, J. Ammonia capture and flexible transformation of M-2(INA) (M=Cu, Co, Ni, Cd) series materials. *J. Hazard. Mater.* **306**, 340–347 (2016).
127. Barea, E., Montoro, C. & Navarro, J. A. R. Toxic gas removal – metal–organic frameworks for the capture and degradation of toxic gases and vapours. *Chem. Soc. Rev.* **43**, 5419–5430 (2014).
128. Decoste, J. B. & Peterson, G. W. Metal–organic frameworks for air purification of toxic chemicals. *Chem. Rev.* **114**, 5695–5727 (2014).
129. NIOSH. Immediately Dangerous to Life or Health Concentrations (IDLH): Ammonia. *The National Institute for Occupational Safety and Health* https://www.cdc.gov/niosh/idlh/7664417.html (1994).
130. Woellner, M. et al. Adsorption and detection of hazardous trace gases by metal–organic frameworks. *Adv. Mater.* **30**, 1704679 (2018).
131. Godfrey, H. G. W. et al. Ammonia storage by reversible host–guest site exchange in a robust metal–organic framework. *Angew. Chem. Int. Ed.* 57, 14778–14781 (2018).
132. Petit, C. et al. Toward understanding reactive adsorption of ammonia on Cu-MOF/graphite oxide nanocomposites. *Langmuir* **27**, 13043–13051 (2011).
133. Kajiwara, T. et al. A systematic study on the stability of porous coordination polymers against ammonia. *Chem. Eur. J.* **20**, 15611–15617 (2014).
134. DeCoste, J. B., Denny, Jr., M. S., Peterson, G. W., Mahle, J. J. & Cohen, S. M. Enhanced aging properties of HKUST-1 in hydrophobic mixed-matrix membranes for ammonia adsorption. *Chem. Sci.* **7**, 2711–2716 (2016).
135. Grant Glover, T., Peterson, G. W., Schindler, B. J., Britt, D. & Yaghi, O. MOF-74 building unit has a direct impact on toxic gas adsorption. *Chem. Eng. Sci.* **66**, 163–170 (2011).
136. Katz, M. J. et al. High volumetric uptake of ammonia using Cu-MOF-74/Cu-CPO-27. *Dalton Trans.* **45**, 4150–4153 (2016).
137. Britt, D., Tranchemontagne, D. & Yaghi, O. M. Metal-organic frameworks with high capacity and

selectivity for harmful gases. *Proc. Natl. Acad. Sci. USA* **105**, 11623–11627 (2008).
138. Petit, C. & Bandosz, T. J. Enhanced adsorption of ammonia on metal–organic framework/graphite oxide composites: analysis of surface interactions. *Adv. Funct. Mater.* **20**, 111–118 (2010).
139. Spanopoulos, I., Xydias, P., Malliakas, C. D. & Trikalitis, P. N. A straight forward route for the development of metal–organic frameworks functionalized with aromatic –OH groups: synthesis, characterization, and gas (N_2, Ar, H_2, CO_2, CH_4, NH_3) sorption properties. *Inorg. Chem.* **52**, 855–862 (2013).
140. Jasuja, H., Peterson, G. W., Decoste, J. B., Browe, M. A. & Walton, K. S. Evaluation of MOFs for air purification and air quality control applications: Ammonia removal from air. *Chem. Eng. Sci.* **124**, 118–124 (2015).
141. Joshi, J. N., Garcia-Gutierrez, E. Y., Moran, C. M., Deneff, J. I. & Walton, K. S. Engineering copper carboxylate functionalities on water stable metal–organic frameworks for enhancement of ammonia removal capacities. *J. Phys. Chem. C* **121**, 3310–3319 (2017).
142. Morris, W., Doonan, C. J. & Yaghi, O. M. Postsynthetic modification of a metal–organic framework for stabilization of a hemiaminal and ammonia uptake. *Inorg. Chem.* **50**, 6853–6855 (2011).
143. Wilcox, O. T. et al. Acid loaded porphyrin-based metal–organic framework for ammonia uptake. *Chem. Commun.* **51**, 14989–14991 (2015).
144. Van Humbeck, J. F. et al. Ammonia capture in porous organic polymers densely functionalized with Brønsted acid groups. *J. Am. Chem. Soc.* **136**, 2432–2440 (2014).
145. Takahashi, A. et al. Historical pigment exhibiting ammonia gas capture beyond standard adsorbents with adsorption sites of two kinds. *J. Am. Chem. Soc.* **138**, 6376–6379 (2016).
146. Doonan, C. J., Tranchemontagne, D. J., Glover, T. G., Hunt, J. R. & Yaghi, O. M. Exceptional ammonia uptake by a covalent organic framework. *Nat. Chem.* **2**, 235–238 (2010).
147. Barin, G. et al. Highly effective ammonia removal in a series of Brønsted acidic porous polymers: investigation of chemical and structural variations. *Chem. Sci.* **8**, 4399–4409 (2017).
148. Vikrant, K., Kumar, V., Ok, Y. S., Kim, K.-H. & Deep, A. Metal-organic framework (MOF)-based advanced sensing platforms for the detection of hydrogen sulfide. *TrAC Trends Anal. Chem.* **105**, 263–281 (2018).
149. Yassine, O. et al. H_2S sensors: fumarate-based fcu-MOF thin film grown on a capacitive interdigitated electrode. *Angew. Chem. Int. Ed.* **55**, 15879–15883 (2016).
150. Wan, X., Wu, L., Zhang, L., Song, H. & Lv, Y. Novel metal-organic frameworks-based hydrogen sulfide cataluminescence sensors. *Sens. Actuators B Chem.* **220**, 614–621 (2015).
151. Petit, C., Levasseur, B., Mendoza, B. & Bandosz, T. J. Reactive adsorption of acidic gases on MOF/graphite oxide composites. *Microporous Mesoporous Mater.* **154**, 107–112 (2012).
152. Petit, C., Mendoza, B. & Bandosz, T. J. Hydrogen sulfide adsorption on MOFs and MOF/graphite oxide composites. *ChemPhysChem* **11**, 3678–3684 (2010).
153. Nickerl, G. et al. Integration of accessible secondary metal sites into MOFs for H_2S removal. *Inorg. Chem. Front.* **1**, 325–330 (2014).
154. Joshi, J. N. et al. Probing metal–organic framework design for adsorptive natural gas purification. *Langmuir* **34**, 8443–8450 (2018).
155. Sánchez-González, E. et al. Highly reversible sorption of H_2S and CO_2 by an environmentally friendly Mg-based MOF. *J. Mater. Chem. A* **6**, 16900–16909 (2018).
156. Belmabkhout, Y. et al. Natural gas upgrading using a fluorinated MOF with tuned H_2S and CO_2 adsorption selectivity. *Nat. Energy* **3**, 1059–1066 (2018).
157. Cadiau, A., Adil, K., Bhatt, P. M., Belmabkhout, Y. & Eddaoudi, M. A metal-organic framework-based splitter for separating propylene from propane. *Science* **353**, 137–140 (2016).
158. Liu, G. et al. Enabling fluorinated MOF-based membranes for simultaneous removal of H_2S and CO_2 from natural gas. *Angew. Chemie Int. Ed.* **57**, 14811–14816 (2018).
159. Subramanian, S. & Zaworotko, M. J. Porous solids by design: $[Zn(4,4'\text{-bpy})_2(SiF_6)]_n \cdot x$DMF, a single framework octahedral coordination polymer with large square channels. *Angew. Chem. Int. Ed.* **34**, 2127–2129 (1995).
160. Cadiau, A. et al. Hydrolytically stable fluorinated metal-organic frameworks for energy-efficient dehydration. *Science* **356**, 731–735 (2017).
161. Mohideen, M. I. H. et al. A fine-tuned MOF for gas and vapor separation: a multipurpose adsorbent for acid gas removal, dehydration, and BTX sieving. *Chem* **3**, 822–833 (2017).
162. Córdoba, P. Status of flue gas desulphurisation (FGD) systems from coal-fired power plants: Overview of the physic-chemical control processes of wet limestone FGDs. *Fuel* **144**, 274–286 (2015).
163. EPA. Power Plant Data Highlights. *US Environmental Protection Agency* https://www.epa.gov/airmarkets/coal-fired-power-plant-data (2018).
164. Ding, L. & Yazaydin, A. O. The effect of SO_2 on CO_2 capture in zeolitic imidazolate frameworks. *Phys. Chem. Chem. Phys.* **15**, 11856–11861 (2013).
165. Pacciani, R. et al. Influence of the concentration of CO_2 and SO_2 on the absorption of CO_2 by a lithium orthosilicate-based absorbent. *Environ. Sci. Technol.* **45**, 7083–7088 (2011).
166. Han, X., Yang, S. & Schröder, M. Porous metal–organic frameworks as emerging sorbents for clean air. *Nat. Rev. Chem.* **3**, 108–118 (2019).
167. Mounfield, W. P. et al. Synergistic effects of water and SO_2 on degradation of MIL-125 in the presence of acid gases. *J. Phys. Chem. C* **120**, 27230–27240 (2016).
168. Yang, S. et al. Irreversible network transformation in a dynamic porous host catalyzed by sulfur dioxide. *J. Am. Chem. Soc.* **135**, 4954–4957 (2013).
169. Yang, S. et al. Selectivity and direct visualization of carbon dioxide and sulfur dioxide in a decorated porous host. *Nat. Chem.* **4**, 887–894 (2012). **Report of the structural visualization of CO_2 and SO_2 within MOF pores, providing insight into the mechanism of selectivity towards SO_2.**
170. Li, L. et al. Post-synthetic modulation of the charge distribution in a metal–organic framework for optimal binding of carbon dioxide and sulfur dioxide. *Chem. Sci.* **10**, 1472–1482 (2019).
171. Tan, K. et al. Mechanism of preferential adsorption of SO_2 into two microporous paddle wheel frameworks $M(bdc)(ted)_{0.5}$. *Chem. Mater.* **25**, 4653–4662 (2013).
172. Cui, X. et al. Ultrahigh and selective SO_2 uptake in inorganic anion-pillared hybrid porous materials. *Adv. Mater.* **29**, 1606929 (2017).
173. Tchalala, M. R. et al. Fluorinated MOF platform for selective removal and sensing of SO_2 from flue gas and air. *Nat. Commun.* **10**, 1328 (2019).
174. Rodríguez-Albelo, L. M. et al. Selective sulfur dioxide adsorption on crystal defect sites on an isoreticular metal organic framework series. *Nat. Commun.* **8**, 14457 (2017).
175. Bhattacharyya, S. et al. Interactions of SO_2-containing acid gases with ZIF-8: structural changes and mechanistic investigations. *J. Phys. Chem. C* **120**, 27221–27229 (2016).
176. Wang, C. et al. Agriculture is a major source of NO_x pollution in California. *Sci. Adv.* **4**, eaao3477 (2018).
177. EPA. Control of Air Pollution from Motor Vehicles: Tier 3 Motor Vehicle Emission and Fuel Standards. *US Environmental Protection Agency* http://www.gpo.gov/fdsys/pkg/FR-2014-04-28/pdf/2014-06954.pdf (2014).
178. The European Commission. Commission Regulation (EU) No 459/2012. *Official Journal of the European Union* http://data.europa.eu/eli/reg/2012/459/oj (2012).
179. Wang, P. et al. Porous metal–organic framework MIL-100(Fe) as an efficient catalyst for the selective catalytic reduction of NO_x with NH_3. *RSC Adv.* **4**, 48912–48919 (2014).
180. Jiang, H. et al. Effect of cosolvent and temperature on the structures and properties of Cu-MOF-74 in low-temperature NH_3-SCR. *Ind. Eng. Chem. Res.* **56**, 3542–3550 (2017).
181. Zhang, M., Wang, W. & Chen, Y. Theoretical investigation of selective catalytic reduction of NO on MIL-100-Fe. *Phys. Chem. Chem. Phys.* **20**, 2211–2219 (2018).
182. Granger, P. & Parvulescu, V. I. Catalytic NO_x abatement systems for mobile sources: from three-way to lean burn after-treatment technologies. *Chem. Rev.* **111**, 3155–3207 (2011).
183. Bartok, W. & Sarofim, A. F. (eds) *Fossil Fuel Combustion: A Source Book*. (Wiley-Interscience, 1991).
184. van Faassen, E. & Vanin, A. *Radicals for Life. The Various Forms of Nitric Oxide*. (Elsevier, 2007).
185. Keefer, L. K. Thwarting thrombus. *Nat. Mater.* **2**, 357–358 (2003).
186. Baudron, S. A. Dipyrrin based homo- and hetero-metallic infinite architectures. *CrystEngComm* **12**, 2288–2295 (2010).
187. Xiao, B. et al. High-capacity hydrogen and nitric oxide adsorption and storage in a metal–organic framework. *J. Am. Chem. Soc.* **129**, 1203–1209 (2007).
188. Wright, A. M., Wu, G. & Hayton, T. W. Structural characterization of a copper nitrosyl complex with a $\{CuNO\}^{10}$ configuration. *J. Am. Chem. Soc.* **132**, 14336–14337 (2010).
189. Bordiga, S. et al. Interaction of N_2, CO and NO with Cu-exchanged ETS-10: a compared FTIR study with other Cu-zeolites and with dispersed Cu_2O. *Catal. Today* **70**, 91–105 (2001).
190. Peikert, K. et al. Tuning the nitric oxide release behavior of amino functionalized HKUST-1. *Microporous Mesoporous Mater.* **216**, 118–126 (2015).
191. McKinlay, A. C. et al. Nitric oxide adsorption and delivery in flexible MIL-88(Fe) metal–organic frameworks. *Chem. Mater.* **25**, 1592–1599 (2013).
192. Bonino, F. et al. Local structure of CPO-27-Ni metallorganic framework upon dehydration and coordination of NO. *Chem. Mater.* **20**, 4957–4968 (2008).
193. McKinlay, A. C. et al. Exceptional behavior over the whole adsorption-storage-delivery cycle for NO in porous metal organic frameworks. *J. Am. Chem. Soc.* **130**, 10440–10444 (2008).
194. Cattaneo, D. et al. Tuning the nitric oxide release from CPO-27 MOFs. *RSC Adv.* **6**, 14059–14067 (2016).
195. Bloch, E. D. et al. Gradual release of strongly bound nitric oxide from $Fe_2(NO)_2(dobdc)$. *J. Am. Chem. Soc.* **137**, 3466–3469 (2015).
196. Ebrahim, A. M., Levasseur, B. & Bandosz, T. J. Interactions of NO_2 with Zr-based MOF: effects of the size of organic linkers on NO_2 adsorption at ambient conditions. *Langmuir* **29**, 168–174 (2013).
197. Peterson, G. W., Mahle, J. J., Decoste, J. B., Gordon, W. O. & Rossin, J. A. Extraordinary NO_2 removal by the metal–organic framework UiO-66-NH_2. *Angew. Chem. Int. Ed.* **55**, 6235–6238 (2016).
198. Han, X. et al. Reversible adsorption of nitrogen dioxide within a robust porous metal–organic framework. *Nat. Mater.* **17**, 691–696 (2018). **The first report of a MOF with reversible capture of NO_2, which forms helical monomer–dimer chains within the pores.**
199. Schulz, M. et al. A calixarene-based metal–organic framework for highly selective NO_2 detection. *Angew. Chem. Int. Ed.* **57**, 12961–12965 (2018).
200. Sava, D. F. et al. Capture of volatile iodine, a gaseous fission product, by zeolitic imidazolate framework-8. *J. Am. Chem. Soc.* **133**, 12398–12401 (2011).
201. Sava, D. F. et al. Competitive I_2 sorption by Cu-BTC from humid gas streams. *Chem. Mater.* **25**, 2591–2596 (2013).
202. Falaise, C. et al. Capture of iodine in highly stable metal–organic frameworks: a systematic study. *Chem. Commun.* **49**, 10320–10322 (2013).
203. Yao, R.-X., Cui, X., Jia, X.-X., Zhang, F.-Q. & Zhang, X.-M. A luminescent zinc(II) metal–organic framework (MOF) with conjugated π-electron ligand for high iodine capture and nitro-explosive detection. *Inorg. Chem.* **55**, 9270–9275 (2016).
204. Li, B. et al. Capture of organic iodides from nuclear waste by metal-organic framework-based molecular traps. *Nat. Commun.* **8**, 485 (2017).
205. Zhang, X. et al. Confinement of iodine molecules into triple-helical chains within robust metal–organic frameworks. *J. Am. Chem. Soc.* **139**, 16289–16296 (2017).
206. Lobanov, S. S. et al. Iodine in metal–organic frameworks at high pressure. *J. Phys. Chem. A* **122**, 6109–6117 (2018).
207. Banerjee, D. et al. Iodine adsorption in metal organic frameworks in the presence of humidity. *ACS Appl. Mater. Interfaces* **10**, 10622–10626 (2018).
208. DeCoste, J. B., Browe, M. A., Wagner, G. W., Rossin, J. A. & Peterson, G. W. Removal of chlorine gas by an amine functionalized metal–organic framework via electrophilic aromatic substitution. *Chem. Commun.* **51**, 12474–12477 (2015).
209. Tulchinsky, Y. et al. Reversible capture and release of Cl_2 and Br_2 with a redox-active metal–organic framework. *J. Am. Chem. Soc.* **139**, 5992–5997 (2017). **Report of a cobalt triazolate framework that oxidatively captures Cl_2 and Br_2 at room temperature and reductively releases them upon heating.**

210. Brozek, C. K. & Dincă, M. Lattice-imposed geometry in metal–organic frameworks: lacunary Zn_4O clusters in MOF-5 serve as tripodal chelating ligands for Ni^{2+}. *Chem. Sci.* **3**, 2110–2113 (2012).
211. Brozek, C. K. & Dincă, M. Cation exchange at the secondary building units of metal-organic frameworks. *Chem. Soc. Rev.* **43**, 5456–5467 (2014).
212. Leus, K. et al. Systematic study of the chemical and hydrothermal stability of selected "stable" metal organic frameworks. *Microporous Mesoporous Mater.* **226**, 110–116 (2016).
213. Richens, D. T. Ligand substitution reactions at inorganic centers. *Chem. Rev.* **105**, 1961–2002 (2005).
214. Helm, L. & Merbach, A. E. Inorganic and bioinorganic solvent exchange mechanisms. *Chem. Rev.* **105**, 1923–1960 (2005).
215. Ripin, D. H. & Evans, D. A. Evans pKa Table. *The Evans Group*. http://evans.rc.fas.harvard.edu/pdf/evans_pKa_table.pdf (2005).
216. Yuhas, B. D., Mowat, J. P. S., Miller, M. A. & Sinkler, W. AlPO-78: a 24-layer ABC-6 aluminophosphate synthesized using a simple structure-directing agent. *Chem. Mater.* **30**, 582–586 (2018).
217. Huberty, M. S., Wagner, A. L., McCormick, A. & Cussler, E. Ammonia absorption at haber process conditions. *AIChE J.* **58**, 3526–3532 (2012).
218. Petit, C., Mendoza, B. & Bandosz, T. J. Reactive adsorption of ammonia on Cu-based MOF/graphene composites. *Langmuir* **26**, 15302–15309 (2010).
219. Savage, M. et al. Selective adsorption of sulfur dioxide in a robust metal–organic framework material. *Adv. Mater.* **28**, 8705–8711 (2016).
220. Fernandez, C. A. et al. Gas-induced expansion and contraction of a fluorinated metal–organic framework. *Cryst. Growth Des.* **10**, 1037–1039 (2010).
221. Mon, M. et al. A post-synthetic approach triggers selective and reversible sulphur dioxide adsorption on a metal–organic framework. *Chem. Commun.* **54**, 9063–9066 (2018).

Acknowledgements
Studies of small-molecule interactions with metal nodes in MOFs are supported through a CAREER grant from the US National Science Foundation to M.D. (DMR-1452612). A.J.R. is supported by the Martin Family Fellowship for Sustainability. The authors thank the Abdul Latif Jameel World Water and Food Security Lab for seed funding for water capture.

Author contributions
A.J.R. and A.M.W. wrote the initial manuscript. A.J.R. and M.D. revised and edited the manuscript prior to submission.

Competing interests
The authors declare no competing interests.

Publisher's note
Springer Nature remains neutral with regard to jurisdictional claims in published maps and institutional affiliations.

RELATED LINKS
US Environmental Protection Agency Sulfur Dioxide Trends: https://www.epa.gov/air-trends/sulfur-dioxide-trends
US Occupational Safety and Health Administration Hydrogen Sulfide: https://www.osha.gov/SLTC/hydrogensulfide/index.html